5-2015

Synthesis and Characterization of Rhodium Acetate with Functionalized Benzonitriles

Jared M. Lowe

Follow this and additional works at: https://dc.etsu.edu/honors

 Part of the Inorganic Chemistry Commons

Abstract

Dirhodium complexes are effective catalysts in carbene transformations. These reactions involve chemistry between the catalyst and a carbene generated *in situ*. In order to better understand the rhodium-carbon bond, studies of rhodium acetate, $Rh_2(OAc)_4$, and a variety of functionalized benzonitriles were proposed. Diadducts of rhodium acetate with 4-nitrobenzonitrile, 4-aminobenzonitrile, 4-(dimethylamino)benzonitrile, and 3,5-dinitrobenzonitrile were successfully prepared and characterized by X-ray crystallography. IR and NMR spectroscopy were also employed for characterization purposes.

Table of Contents

List of Figures

List of Tables

1. Introduction

1.1 The Dirhodium Complex

Much research has been produced in the development of dirhodium complexes as organic catalysts.[1] Since the 1970s, the uniquely paddlewheeled structure of rhodium acetate, $Rh_2(OAc)_4$, has been known to catalyze decomposition of ethyl diazoacetate, as discovered by the Teyssie group.[2] The crowning achievement of dirhodium catalysts, however, are metal carbene transformations, which include carbon-hydrogen insertion, cyclopropanation, cyclopropenation, and ylide transformations.[3] These reactions are not only of academic interest, but have successful industrial, pharmaceutical and agricultural applications.

The paddlewheeled structure of the dirhodium complex is created when four bridging ligands bond to both rhodium atoms. These ligands include carboxylates, perfluorinated carboxylates, and carboxamidates, to name a few. For example, dirhodium(II) carboxylates, such as tetrakis(μ-acetato)dirhodium(II), or rhodium acetate, involve the two rhodium atoms bound together in a 2+ oxidation state, while the bridging ligands, here, acetate groups, have a -1 charge.
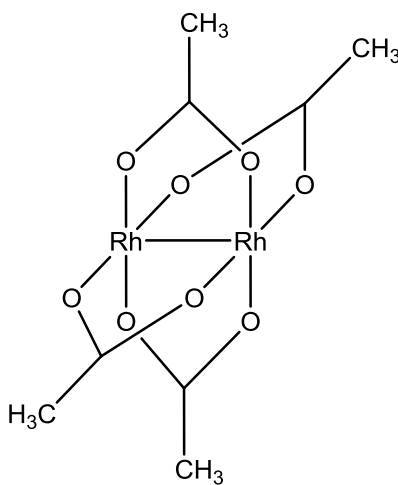
Figure 1: Structure of tetrakis(μ-acetato)dirhodium(II), or rhodium acetate.

While rhodium acetate was the jumping off point for catalytic investigations, carboxylates and perfluorinated carboxylates lack stereoselective control in cases where diastereomeric products are formed. The placement of chiral ligands on the dirhodium(II) core has been seen to create asymmetric complexes with increased selectivity. Efforts to create these asymmetric catalysts began with the addition of *N*-protected amino acids, such as prolinate, and have shown high selectivity in C-H insertions.[4]

The development of dirhodium(II) carboxamidates has provided a wider variety in stereospecificity than the chiral carboxylates. The chiral carboxamidate ligand bridges the dirhodium core unsymmetrically: oxygen bonds to one rhodium and nitrogen to the other. This leads to four possible isomers in this class of dirhodium complex: *cis*-(2,2), *trans*-(2,2), (3,1)-, and (4,0)-.
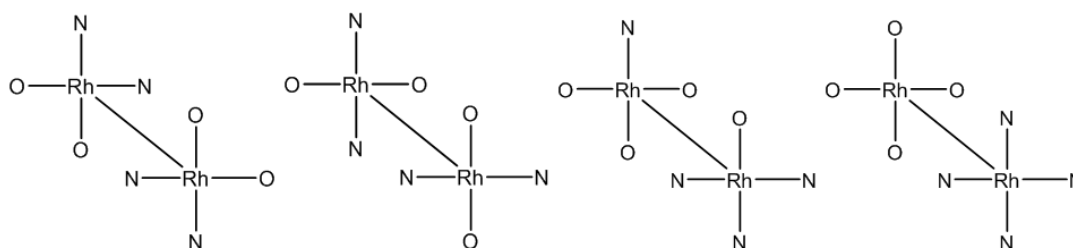
Figure 2: (from left to right) The *cis*-(2,2), *trans*-(2,2), (3,1)-, and (4,0)- isomers of dirhodium(II) carboxamidates.

Synthesis of dirhodium(II) carboxamidates began with isolation of dirhodium(II) tetraacetamide from rhodium acetate in a melt of acetamide.[5] More complex carboxamidates were able to be used by trapping the released acetic acid by a Soxhlet extractor. At first, cyclic amides were used as chiral carboxamidate ligands because rotation about the nitrogen atom hindered ligand exchange.[6] However, acetanilide (*N*-phenylacetamide) is a suitable, acyclic amide that can successfully exchange the acetate ligand from the dirhodium(II) core.

That being said, the synthesis of dirhodium(II) carboxamidates is a difficult and time-consuming process and purification of this complex is often difficult.[7] Therefore, it is useful to exploit rhodium acetate where possible in order to save time and money.

1.2 Carbene Transformations

Originally suggested by Yates for copper catalysts, it is now accepted that transition metal catalysts react with diazo compounds to generate transient electrophilic metal carbenes.[8,9] The catalytic activity of the complexes depends on coordinative unsaturation at the metal center. Electrophilic addition causes loss of dinitrogen and produces a metal stabilized carbene. The carbene then reacts with an electron rich substrate, completing the catalytic cycle.
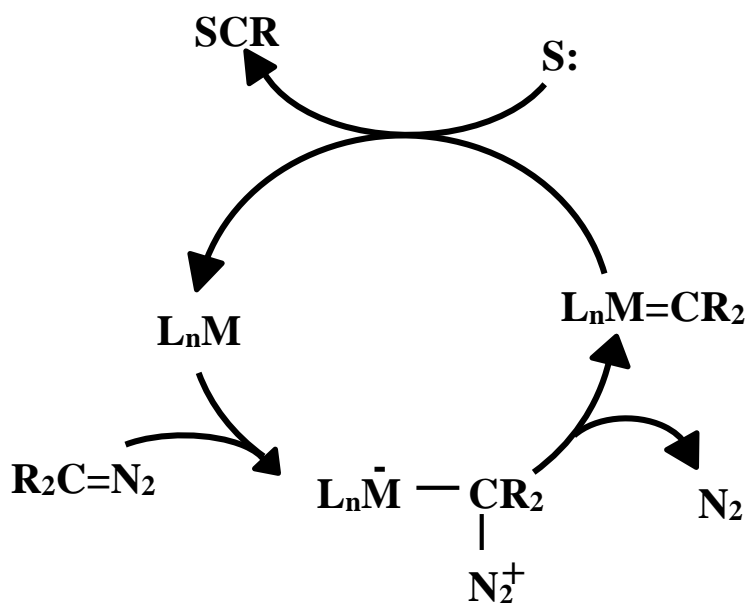
Figure 3: Catalytic cycle of decomposition of diazo compounds.

Catalysts that can perform this reaction include insoluble copper bronze and cupric sulfate; soluble bis(acetylacetonato)copper(II); copper triflate (trifluoromethanesulfonate); and even palladium complexes such as palladium(II) acetate. However, rhodium acetate has been

8

shown to be a superior catalyst for many carbenoid transformations and rhodium acetate as a cyclopropanation catalyst consistently produces high yields of cyclopropane products throughout the spectrum of olefin reactivities.[9]

Table 1: Cyclopropanation of olefins by various catalysts.[9]					
Olefin/diazo compound	Product	Heterogeneous catalyst	Yield	Homogeneous catalyst	Yield
		Cu, Et$_2$O, reflux	66%	Rh$_2$(OAc)$_4$, 25 °C	90%
		Cu 100-130 °C	64%	Rh$_2$(OAc)$_4$, 20 °C	85%
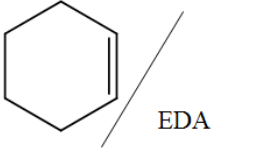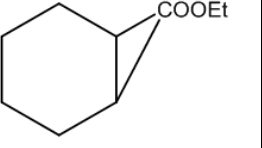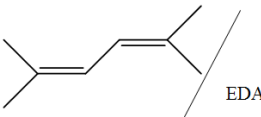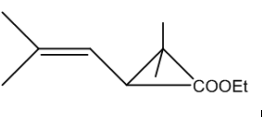
The mechanism of cyclopropanation for these catalysts has been investigated through study of reactivity-selectivity correlations of diazo compounds and olefins in the presence of dirhodium and tungsten complexes. When benzylidine was the diazo compound used, *cis*-cyclopropanes were produced and when ethyl diazoacetate was used, *trans*-cyclopropanes were produced. In order to explain the *trans*-cyclopropane, a discrete metallocycle was proposed by Casey and co-workers during their initial investigations.[10] This was reinforced by observation that as the size of the R group was increased, the *trans*-isomer is the preferred product.
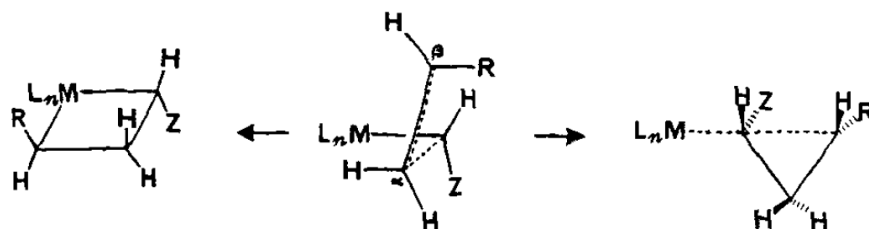
Figure 4: Proposed cyclopropanation mechanism by Casey.[10]

While the pathway above accounts for stereochemistry of cyclopropane formation, this model does not explain selectivity for all diazo compounds. Doyle and co-workers therefore

proposed an alternate mechanistic model. First, the olefin associates through its π-bond with the

electrophilic center of the metal-carbene complex. The catalyst is displaced by σ-bond formation.

Stabilization of the electrophilic center by the electron donating substituent, R, determines the

motion of the olefin relative to the carbene. To form the *cis*-isomer, the olefin moves up and

rotates to the T_c configuration. For the *trans*-isomer the olefin moves down and rotates to the T_t

configuration. Stereochemistry here is determined by a combination of steric and electronic

interactions.
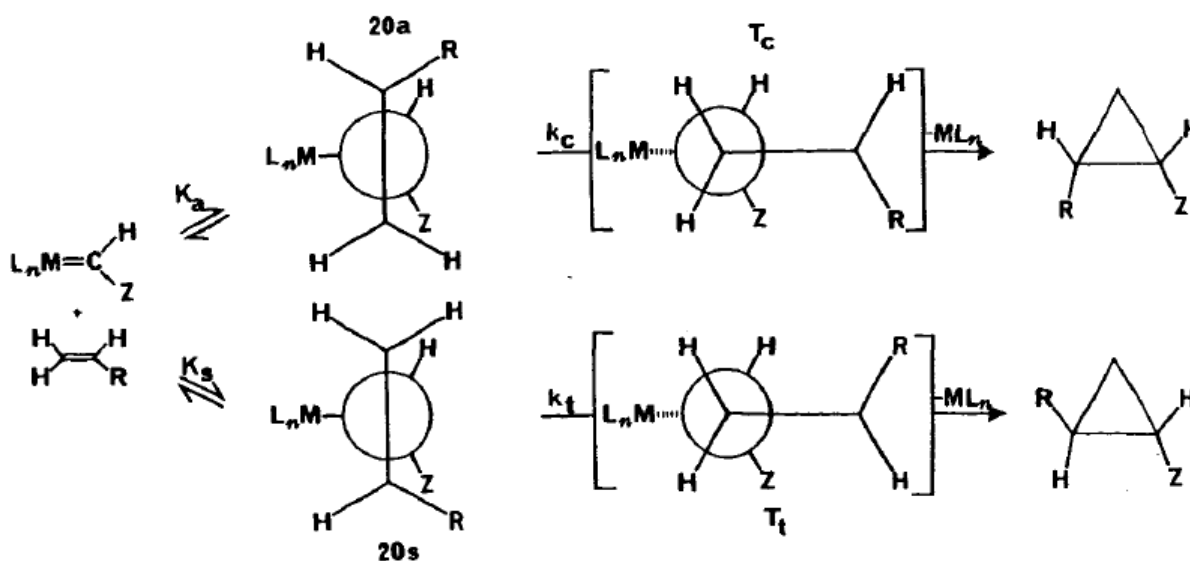
Figure 5: Proposed cyclopropanation mechanism by Doyle.[9]

Cyclopropanes are commercially useful, and their stereospecificity is of great importance.

One specific application is the formation of pyrethroid insecticides. The active part of this

molecule is a *cis*-cyclopropane ring catalyzed by the complex from a carbene and an alkene. This

type of insecticide is harmless to humans and other animals and thus it is used in bug repellants

and pet care products. As mentioned in Section 1.1, changing the equatorial ligands on the

dirhodium core can affect a large change in the stereospecificity in the catalytic reactions.

While the rhodium complex's application in carbene chemistry catalysis has been achieved, the bonding process between the carbene and the rhodium is still not completely understood. The rhodium stabilized carbene reacts very quickly, and has not been observed. In order to better understand this organometallic bond, and to create more efficient catalysts in the future, the purpose of this research is to make use of a stable analog to probe the catalytic site of rhodium acetate.

1.3 Nitriles as Carbene Analogs

Before a discussion of carbene analogs, it is useful to introduce molecular orbitals of dirhodium species. First, the dirhodium core has fourteen electrons available for bonding, with each rhodium atom contributing seven electrons in d orbitals. There are five types of d orbitals, differentiated by the Cartesian coordinates found in the solutions to the Schrödinger equation and are as follows: d_{xy}, d_{xz}, d_{yz}, $d_{x^2-y^2}$, and d_{z^2}. Each orbital has a different configuration in space, and therefore interacts differently to each other when in close contact.

In order to make discussion on the rhodium to rhodium interaction clear, the *z*-axis will be designated as the axis of internuclear interaction. Because of this designation, the two d_{z^2} orbitals can combine end-on for σ-bonding, named so because the resulting orbital is symmetric to rotation about the line connecting the nuclei.[11] The d_{xz} and d_{yz} orbitals form π orbitals, meaning that they are antisymmetric to 180° rotation about the line of interaction (a C₂ rotation). This is because the orbitals combine in an end to end manner. When atomic orbitals from two parallel planes combine side to side, like the d_{xy} orbital, a δ (delta) orbital is formed, meaning it is antisymmetric to 90° rotation about the line of interaction (a C₄ rotation). The $d_{x^2-y^2}$ orbital also has the ability to form a δ-bond; however, this is unavailable for metal to metal bonding because it is geometrically located where the four equatorial bridging acetate

ligands bond to the dirhodium core. This orbital therefore is used exclusively for metal to ligand

bonding. A pictorial representation of the atomic and subsequent molecular orbitals is given in

Figure 6.

d_{z^2} orbitals
end-to-end

d_{xz} or d_{yz} orbitals
in the same plane

d_{xy} orbitals
($d_{x^2-y^2}$ participates in
M-L bonding only)
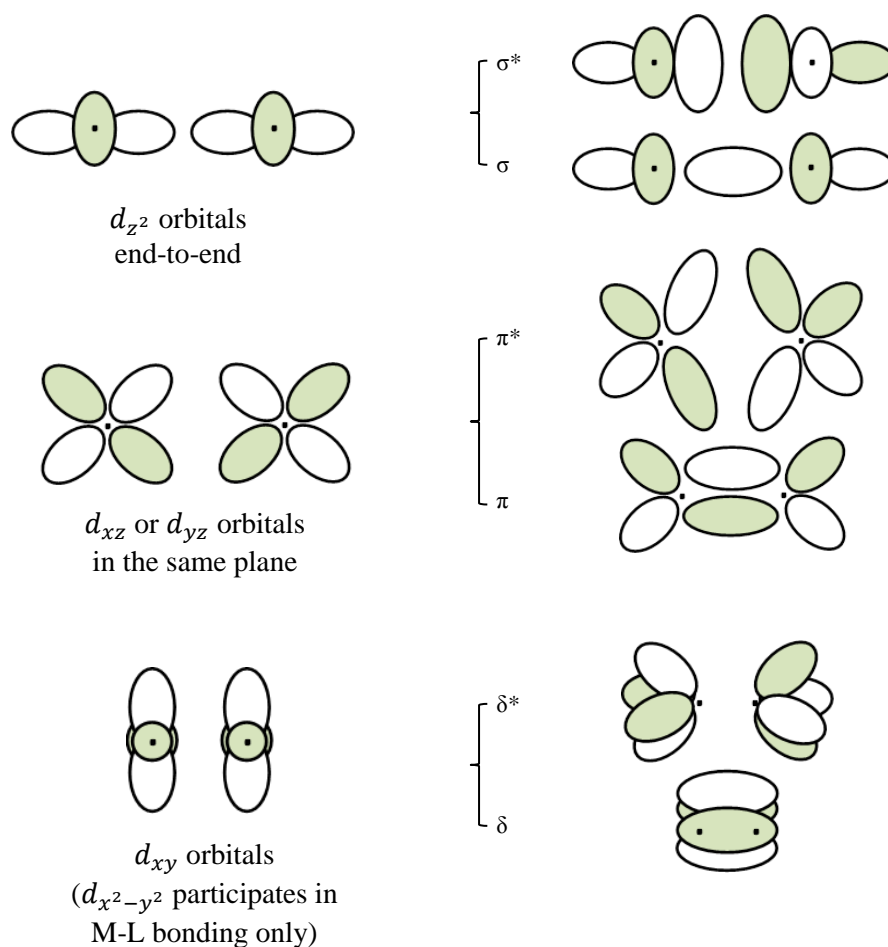
Figure 6: Interactions of *d* orbitals.[11]

A requirement of molecular theory is that for every bonding orbital formed an anti-

bonding orbital is also possible.[11] This is designated by an asterisk (*). Eight of the fourteen

electrons reside in the σ, π, and δ orbitals, while the remaining six occupy the π* and δ* orbitals.

This indicates that the Rh-Rh bond order is one with no unpaired electrons.[12] Note that there is

only one set of empty δ and δ*orbitals in Figure 7. Again, this occurs from orbital overlap and

the orbitals are not available for Rh-Rh bonding. The highest occupied molecular orbital

(HOMO) is δ* and the lowest unoccupied molecular orbital (LUMO) is σ*, meaning that each

rhodium atom can accept a pair of electrons from another molecule in the axial site.
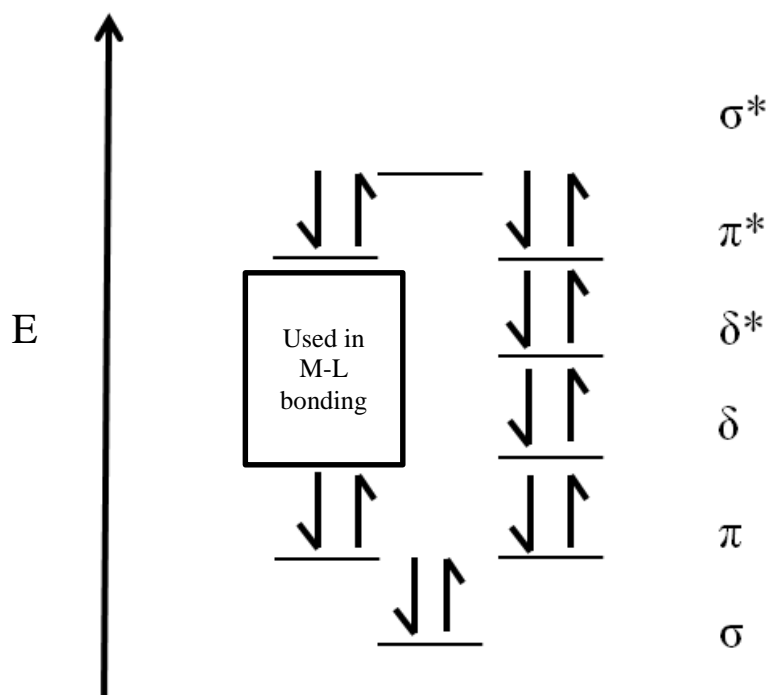
Figure 7: Molecular orbital diagram for the dirhodium(II) core.

Based on this information, it appears that the axial site on the dirhodium complex is able

to accept a pair of electron to form a σ-bond. The electrons in the π* orbitals are also

geometrically available for bonding to the axial ligand, creating a π-bond. Because this π-bond is

created in a direction opposite to the σ-bond, it is referred to as a π-backbond. If this is applied to

a carbene, the σ-bond is created by the lone pair of electrons on the carbon atom. The π-

backbond is created when the electrons from the dirhodium core are donated to the vacant *p* type

orbital on the carbon atom.
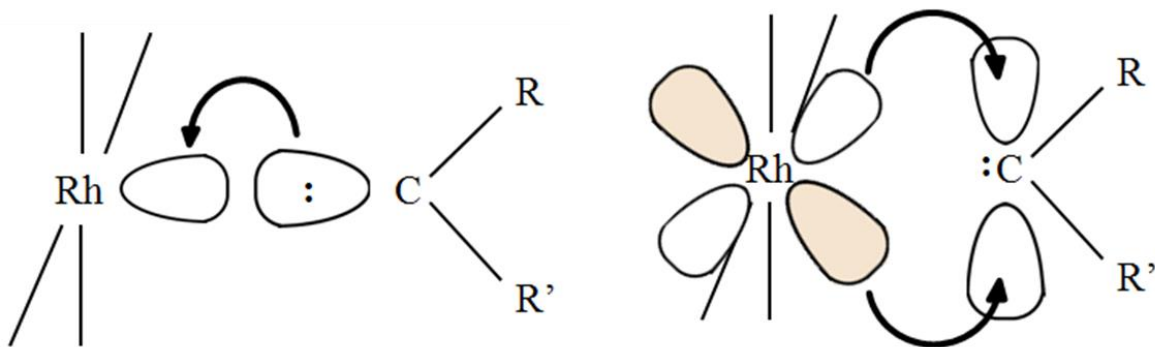
Figure 8: Proposed bond formation between dirhodium(II) complex and carbene.

σ-bonding (left) and π-backbonding (right).

As mentioned in Section 1.2, the rhodium-carbene bond is a transient species and has not been isolated. In order to better understand this bonding process, an analog has been selected to replace the carbene. An analog in this situation must have orbitals similar to a carbene in order to observe both σ-bonding and π-backbonding. This analog must also be more stable than the carbene in order to facilitate characterization. In this research, the proposed analog is a functionalized benzonitrile. Nitriles have a lone pair of electrons on the nitrogen atom, similar to the carbene. Also the nitrogen to carbon triple bond has a vacant π* orbital available for π-backbonding. This orbital is angled more towards the rhodium orbitals than the carbene's p type orbital, so π-backbonding should be more likely to form. Even though this analog has the potential to exhibit the desired bonding, true understanding of the catalytic species is to some extent sacrificed because a benzonitrile cannot perform the reactions of interest as a carbene.

Acetonitrile has been used as an axial ligand for rhodium acetate and was studied by Cotton and co-workers.[13] Also, benzonitrile attached to tetrakis(N-phenylacetamidato)dirhodium(II) has been studied by the Eagle group.[14]

In addition to these structures, isonitriles have been used as axial ligands for rhodium acetate, a work accomplished by the Eagle group.[15] Isonitriles are essentially a "reverse" nitrile,

14

meaning that the carbon atom has the lone pair of electrons and nitrogen is bonded to the hydrocarbon backbone, here, the benzene ring. Isonitriles are not as stable as nitriles and they must be synthesized immediately before use; however, the π^* antibonding orbital for carbon triple bonded to nitrogen has larger lobes on the carbon atom. This could make π-backbonding more energetically possible for the rhodium-carbon bond.

In the isonitrile study, three isonitriles were used: 4-(dimethylamino)phenyl isonitrile, phenyl isonitrile, 4-(trifluoromethyl)phenyl isonitrile.[15] These were selected in order to affect the electronic environment around the isonitrile, a concept that will be explained later in this section. Figure 9 is a thermal ellipsoid plot of the 4-(trifluoromethyl)phenyl isonitrile adduct of rhodium acetate. The authors found that the aromatic rings in the crystal structure were coplanar, which could indicate that conjugation had occurred. Conjugation means that a π molecular orbital is delocalized and spread over many atoms. They asserted that the π-backbond took part in this conjugation. It is currently unknown if this can be extended to benzonitriles as well.
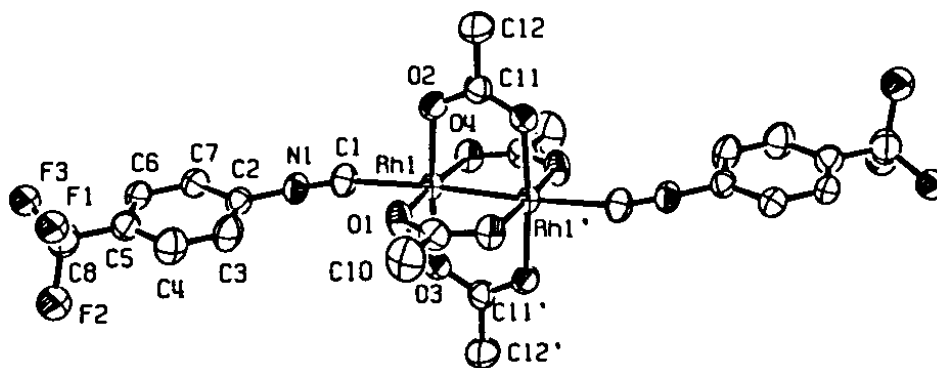
Figure 9: Thermal ellipsoid plot of the 4-(trifluoromethyl)phenyl isonitrile

adduct of rhodium acetate.

For this study, the phenyl ring on the benzonitrile will have various electron donating or electron withdrawing substituents.[16] This could impact the stability of the rhodium-nitrogen bond. Specifically the benzonitriles used for axial ligands are: 4-nitrobenzonitrile, 4-

aminobenzonitrile, 4-(dimethylamino)benzonitrile, 3,5-dinitrobenzonitrile, 3,5-dichlorobenzonitrile, and 3,5-diaminobenzonitrile (Figure 10).
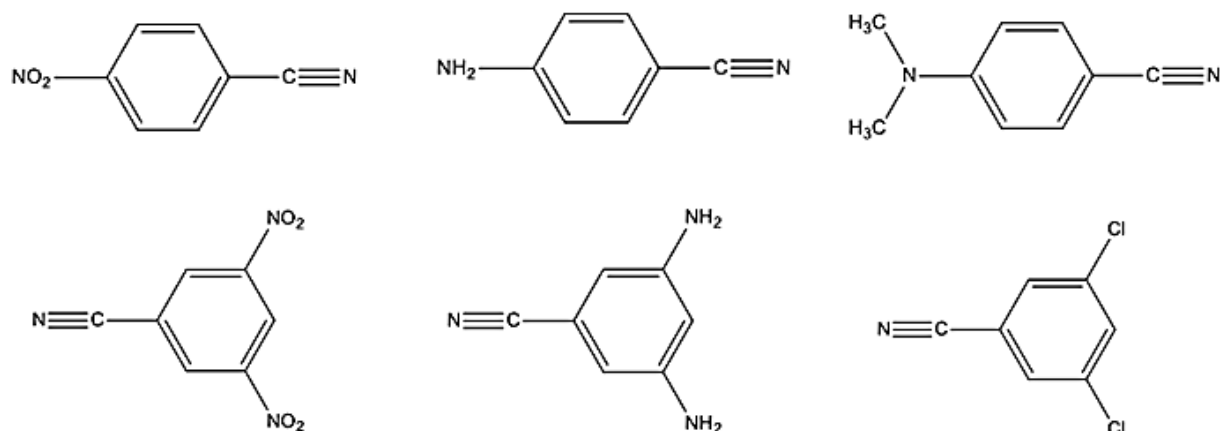
Figure 10: Functionalized benzonitriles, top row: 4-nitrobenzonitrile (left), 4-aminobenzonitrile (center), 4-(dimethylamino)benzonitrile (right), bottom row: 3,5-dinitrobenzonitrile (left), 3,5-diaminobenzonitrile (center), 3,5-dichlorobenzonitrile (right).

While substituents are usually discussed for the reactivity of the benzene ring itself, this can be extended to the electronic effects on nitrile functional group as well. Substituents on the benzene ring of the benzonitrile can withdraw or donate electrons. This is controlled by interplay of inductive and resonance effects.[16] An inductive effect is caused by the withdrawal or donation of electrons through a σ-bond due to a difference in electronegativity between the two bonded atoms. Halogens, hydroxyl groups, carbonyl groups, cyano groups, and nitro groups withdraw electrons inductively while alkyl group donate electrons, similar to carbocation stabilization.

Resonance effects occur through π-bonds when a p-orbital on the substituent overlaps with a p-orbital on the aromatic ring. Carbonyl, cyano, and nitro groups withdraw electrons by resonance leaving a positive charge on the aromatic ring. Halogens, hydroxyl groups, and amino groups donate by resonance because of they all contain a lone pair of electrons.

16

These effects do not always act in the same direction. When the two effects compete with each other, the stronger one predominates.[16] For example, halogens withdraw electrons because of their high electronegativity. Hydroxyl groups and amino groups donate electrons because the resonance effect is stronger than the inductive effect. In this study, the dimethylamino group should also donate electrons because the methyl groups donate inductively and the nitrogen atom can donate by resonance.

1.4 X-ray Crystallography

X-ray crystallography is the central characterization technique for this research. Developed only a century ago, this technique has been used to solve the structures of hundreds of thousands of compounds. Crystallography explores the spatial arrangements of atoms in the unit cell, the repeating unit of atoms in a crystalline structure. From this information, atomic positions, bond lengths, bond angles, and torsion angles can be determined. This will support the determination of π-backbonding in the novel rhodium acetate adducts, as discussed below. But first, a brief introduction to the history and theory of X-ray crystallography is necessary.

In 1895 Wilhelm Röntgen discovered X-rays; however, it was unknown at the time whether or not X-rays were particles or electromagnetic waves. In 1912, Max von Laue at the University of Munich hypothesized that a crystal's periodic structure would be able to diffract X-rays, assuming that crystals were periodic and that X-rays were waves. Von Laue and his colleagues subsequently irradiated a crystal of copper sulfate with X-rays. When a diffraction pattern was observed, the science of X-ray crystallography was born.[17]

Just as in other types of electromagnetic radiation, when X-rays pass through a crystalline solid, the electric component of the radiation interacts with the electrons in the solid's atoms. This scatters the X-rays, which produces constructive and deconstructive interference among the

scattered rays and therefore diffraction. This occurs because the X-ray wavelength is of the same

order of magnitude as the distances between the scattering centers. When a crystal is irradiated

with X-rays at some angle θ, a fraction of the beam is scattered by the atoms at the surface.

Another fraction penetrates through the crystal to another repeated layer of atoms and is then

scattered as well.
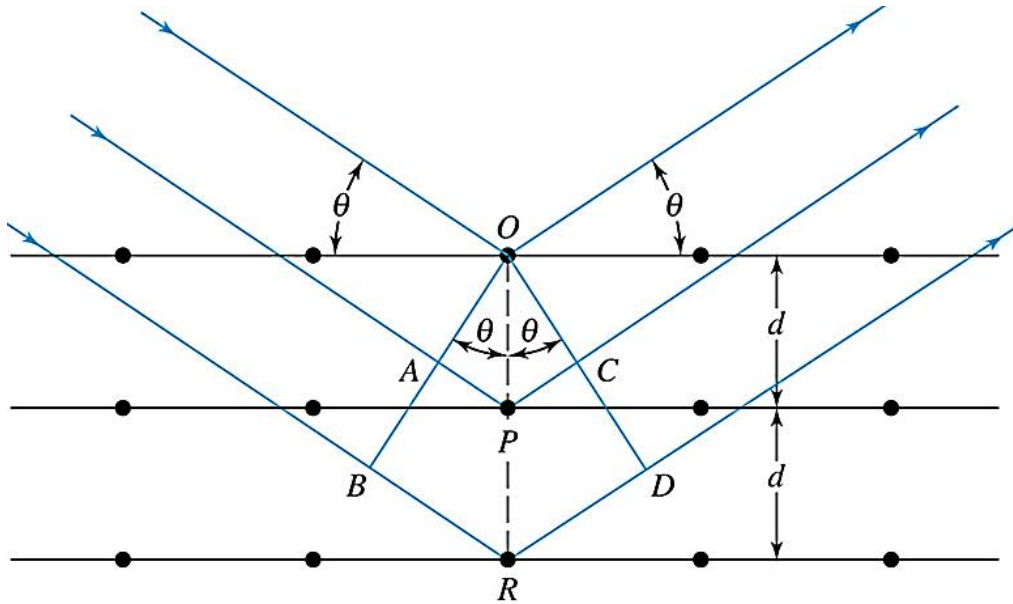
Figure 11: Diffraction of X-rays by a crystal.[18]

Because of this effect, William Lawrence Bragg in 1912 treated the geometry of a crystal

analogously to the reflection of light by a plane mirror. This application led to the derivation of

the now famous Bragg's Law.

$$\mathbf{n}\lambda = 2dsin\theta$$

This formula indicates the conditions for constructive interference of the X-ray beam at angle θ,

where **n** is an integer, λ the wavelength of radiation and *d* the interplanar distance of the

crystal.[18]

In modern diffractometers, a crystal is mounted onto a mitogen loop or glass fiber and

inserted into the instrument. More specifically, it is placed on a goniometer which not only

provides the ability to center the crystal in the X-ray beam but also allows the crystal to rotate in the many directions needed for analysis. When the crystal is irradiated with X-rays, the atoms scatter the radiation, sending the rays in all directions, creating constructive and deconstructive interference as mentioned earlier. This unique diffraction pattern is recorded on a charge coupled device (CCD) camera. The diffraction pattern is dependent upon the size, quality, and thermal vibration of the crystal structure. It is greatly encouraged that the analysis be conducted at low temperatures to reduce the thermal vibration. Using a computer software package, the images produced on the CCD camera are then used to determine the three-dimensional structure of the crystal.

In this structural determination, there are a set of parameters that specify the location of every atom in the unit cell. Use of refinement techniques, such as least squares, automatically adjust these parameters to produce more accurate measurements of atomic position and is used to calculate uncertainties in bond lengths and angles. A measurement of the correctness of a structure is given by the residual or R value

$$R = \frac{\Sigma |F_{observed} - F_{calculated}|}{\Sigma |F_{obserbed}|}$$

Where F is the structure factor, and is related to the intensity of the reflection. An R of 0.20 may indicate a correct structure; however, R should be considerably less than that. An R of 0.10 or lower can be produced if the quality of the crystal and the data were high.[17]

The goodness of fit is another value that describes the quality of a structure, referring to how the model compares to the observed data values. This value should approach unity. Last, if the model is correct, all electron density should be accounted for. This is not entirely possible, however, and maximum and minimum peaks in the final difference map are used to describe the

residual electron density in the model. A negative value in the minimum peak translates to a lack of electron density, or "hole," in the model.

In a description of a crystal, the unit cell can be classified by crystal systems and Bravais lattices based on its symmetry. There are seven crystal systems and fourteen Bravais lattices, as shown in Table 2.[17] For example, the monoclinic crystal system is distinguished by the α and γ angles of the unit cell both equal to 90º. In the monoclinic system, there are two Bravais lattices: primitive and C-centered. In a primitive cell the lattice points, or identical points in all unit cells, are found only in the corners of the unit cell. In a C-centered cell, there are two additional lattice points in center of the C-faces of the unit cell. In other crystal systems, it is possible for unit cells to be body centered, designated by I (from the German, *innenzentriert*); face centered, designated by F; and rhombohedral, designated by R. Bravais lattices are necessary in order to preserve the characteristics of the unit cell on the basis of symmetry. A discussion of the origin of nonstandard centering will not be given here.

Table 2: The seven crystal systems and fourteen Bravais lattices.[17]		
Crystal System	Restrictions on Axes and Angles	Bravais Lattices
Triclinic	None	P
Monoclinic	$\alpha = \gamma = 90°$	P, C
Orthorhombic	$\alpha = \beta = \gamma = 90°$	P, C, I, F
Tetragonal	$a = b$ $\alpha = \beta = \gamma = 90°$	P, I
Trigonal	$a = b = c$ $\alpha = \beta = \gamma = 90°$ or $a = b$ $\alpha = \beta = 90°$ $\gamma = 120°$	R
Hexagonal	$a = b$ $\alpha = \beta = 90°$ $\gamma = 120°$	P
Cubic	$a = b = c$ $\alpha = \beta = \gamma = 90°$	P, I, F

2. Methods

2.1.1 Reagents

- Rhodium acetate is available commercially and was purchased from Pressure Chemical

  Company

- Functionalized benzonitriles (used as supplied):

  4-Nitrobenzonitrile (purchased from Acros Organics)

  4-Aminobenzonitrile (purchased from Acros Organics)

  4-(Dimethylamino)benzonitrile (purchased from Acros Organics)

  3,5-Dinitrobenzonitrile (purchased from Alfa Aesar, A Johnson Matthey Company)

  3,5-Dichlorobenzonitrile (purchased from Enamine)

  3,5-Diaminobenzonitrile (purchased from Aldrich)

- Ethanol was used to dissolve the starting materials in order for the addition reaction to occur.

- The following solvents were used for vapor diffusion study (described in Section 2.2):

hexanes, toluene, methanol, ethyl acetate, acetone, and water.

2.1.2 Instrumentation

- X-ray diffractometer

    Rigaku Mercury 375R/M CCD(XtaLAB mini). Manufactured in 2011.

- NMR spectrometer

    400 MHz JEOL NMR

- IR spectrometer

    Shimadzu IR Prestige-21

2.2 Synthesis and Crystallization

Approximately 10 mg of rhodium acetate was measured on an analytical balance (APX Denver Inst) and transferred into a sample vial. A 10:1 molar excess of a particular benzonitrile was also measured on the analytical balance and also transferred to a separate sample vial. Both compounds were dissolved in 10 mL of ethanol. The rhodium acetate solution was blue green in color and the benzonitrile solutions ranged from colorless to light yellow and brown in color. All solutions were clear and not cloudy. Once dissolved, the benzonitrile solution was added directly to the rhodium acetate solution. Each of the benzonitriles listed above were mixed with rhodium acetate in a similar manner. No immediate color changes were observed upon addition of any benzonitrile, with the exception of 3,5-diaminobenzonitrile, which produced a red, apparently amorphous, precipitate.

Once the addition was completed, a small aliquot (roughly 2-4 mL) of solution was transferred to each of six smaller sample vials. These sample vials were inserted into larger vials each with a different solvent (described in Section 2.1) and then capped. This technique is called vapor diffusion. The outer solvent, often called the precipitant, evaporated and diffused into the

inner solvent. This then led to oversaturation (if the compound of interest was insoluble in the outer solvent), nucleation, and then crystallization. A seventh small vial was not placed in a vapor diffusion vial for crystallization; therefore the crystallization process occurred by slow evaporation.

After one week to two weeks, small, red crystals appeared in a few vials. At this point, some of the vials' caps were replaced with either paraffin wax or a Kimwipe with a few holes in order to evaporate the remaining solvent more rapidly. This was done to promote faster crystallization of the remaining compound in solution and evaporation of the excess solvents. Generally after one additional week, high-quality crystals were obtained from at least one sample vial. While X-ray quality crystals were found in more than one vial in each vapor diffusion setup, only one crystal was structurally determined for each unique adduct.

2.3 Preparations for X-ray Characterization

In order to select a crystal for analysis, the contents of one sample vial were transferred to a microscope slide, on which a thin layer of STP grease was applied. Under the microscope, the crystals were analyzed for imperfections and for desired dimensions (approximately 0.1mm on each axis). If a crystal of proper quality was selected but was too large, the crystal was cut by a small scalpel. Using a small needle, a small amount of Apiezon grease was first applied to the selected crystal and then mounted onto a Mitogen loop. This mitogen loop was then mounted on the goniometer inside the X-ray diffractometer for analysis. Again, all measurements were made on a Rigaku Mercury375R/M CCD (XtaLAB mini) diffractometer using graphite monochromated Mo-Kα radiation. For all data collections, the crystal to detector distance was 50.00 mm. The exposure rate was 10.0 sec./º, and the temperature for all data was set to 223.15 K.

For the adducts that were successfully characterized, the crystals from the bulk product were isolated from the excess ligand. This was performed by separating the adduct (red crystals) from crystallized benzonitrile ligand (colorless crystals) under microscope. Once this was accomplished, the crystals were placed inside an IR spectrometer for analysis. In order to perform NMR analysis for the adducts formed, the crystals used in IR analysis were dissolved in deuterated chloroform ($CDCl_3$)

3. Results and Discussion

3.1 X-ray Crystallography

Of the six unique benzonitrile ligands used in the addition reaction with rhodium acetate, structures of four different adducts were successfully determined by X-ray crystallography at the time of this publication. These $Rh_2(OAc)_4$ adducts contained 4-nitrobenzonitrile, 4-aminobenzonitrile, 4-(dimethylamino)benzonitrile, and 3,5-dinitrobenzonitrile as the axial ligand. All compounds were diadducts. The 3,5-dichlorobenzonitrile adduct did not produce X-ray quality crystals. The 3,5-diaminobenzonitrile adduct produced a red precipitate, presumed to be amorphous. However, after several months, this red precipitate had reentered solution, making the case for a kinetic and thermodynamic product. A crystallization study of this adduct was conducted by another member of the Eagle group.

In many types of reactions, more than one product can form from the same reactants. In order for the reactants to form products, they must absorb energy. This energy is used to break bonds and/or form new ones. The energy change that takes place is referred to as Gibbs free energy-change (ΔG) and can be positive or negative. A favorable reaction has a negative ΔG

value, meaning that total energy after the reaction is lost to the surroundings, and is said to be exergonic. The opposite is true for reactions with positive ΔG values, said to be endergonic.

In between the formation of product from reactant, there is an energy maximum, where the chemical species is least stable. This is called the transition state ($\Delta G\ddagger$), and it is the intermediate of product and reactant. There can be more than one transition state, and they can lead to different products of varying stability. For example, consider a reaction that can form only two products. The first product's transition state is lower than the second's ($\Delta G\ddagger_1 < \Delta G\ddagger_2$) but its free energy change is higher ($\Delta G_1 > \Delta G_2$). Even though the first product is not as stable as the second, it can more easily form. This is called the kinetic product. In the competition to form products, the first product will win and predominate, at least in the short term. As time progresses, however, or if reaction conditions are changed, like pressure or temperature, some of the reactants can obtain enough energy to reach the higher transition state and become the second product. This is referred to as the thermodynamic product. For the situation encountered in this research, it is possible that what is considered to be an insoluble kinetic product formed immediately and the soluble thermodynamic product formed as time progressed. In the future it is recommended to perform this reaction at a higher temperature, in order to observe if the soluble product forms initially.

3.1.1 The 4-nitrobenzonitrile Adduct of $Rh_2(OAc)_4$

The $[Rh_2(COOCH_3)_4] \cdot 2NCC_6H_4NO_2$ crystal was a red prism having approximate dimensions of 0.210 x 0.160 x 0.120 mm mounted on a mitogen loop. The lattice parameters measured for the crystal's unit cell determined that the $[Rh_2(COOCH_3)_4] \cdot 2NCC_6H_4NO_2$ crystal system was innenzentriert (I-centered) and monoclinic. For Z=4 and formula weight equaling

738.24 g/mol, the calculated density was 1.898 g/cm^3. A total of 540 oscillation images were collected.

Table 3: Crystal data for $[Rh_2(COOCH_3)_4]\cdot 2NCC_6H_4NO_2$.	
Empirical Formula	$C_{22}H_{20}N_4O_{12}Rh_2$
Formula Weight	738.24 g/mol
Crystal Dimensions	0.210 x 0.160 x 0.120 mm
Crystal System	Monoclinic
Lattice Type	I-Centered
Lattice Parameters	a = 15.206(2) Å
	b = 9.1212(12) Å
	c = 18.811(3) Å
	β = 98.038(12)º
	V = 2583.4(6) Å^3
Space Group	I12/c1 (#15)
Residuals: R1 (I>2.00σ(I))	0.0262
Residuals: R (All reflections)	0.026
Residuals: wR2 (All reflections)	0.064
Goodness of Fit Indicator	1.044
Max Shift/Error in Final Cycle	0.018
Maximum peak in Final Diff. Map	0.34 e$^-$/Å^3
Minimum peak in Final Diff. Map	-0.98 e$^-$/Å^3

In Figure 12, a thermal ellipsoid plot (TEP) of the adduct is shown. It indicates the probability of the locations of atoms in the unit cell. The larger the ellipsoid, the more likely the atom is in a slightly different position from unit cell to unit cell. This TEP was created in OLEX, a software package used to solve crystal structures. There is a very slight bend in the Rh1-N1-C5 bond angle. Additionally there is a twist in the nitro group, meaning that it is not in the plane of the phenyl ring. The twist is likely due to the intermolecular forces holding the solid state together. In Figure 13, two different interactions can be seen. In the center of the figure, the oxygen atoms that are part of the nitro group (O5 and O6) bend away from a phenyl ring of the adjacent adduct. Two such interactions are observed here. The second interaction involves one oxygen atom in close contact with the methyl carbon on one of the equatorial acetate ligands. This can be seen in the lower right corner of the figure.
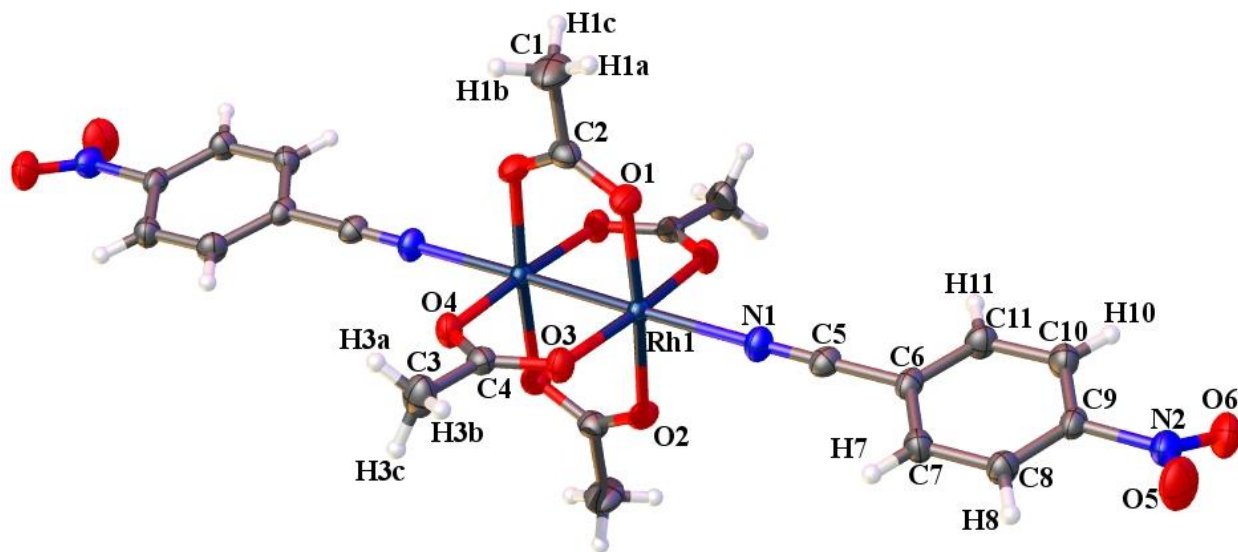
Figure 12: TEP of 4-nitrobenzonitrile adduct.
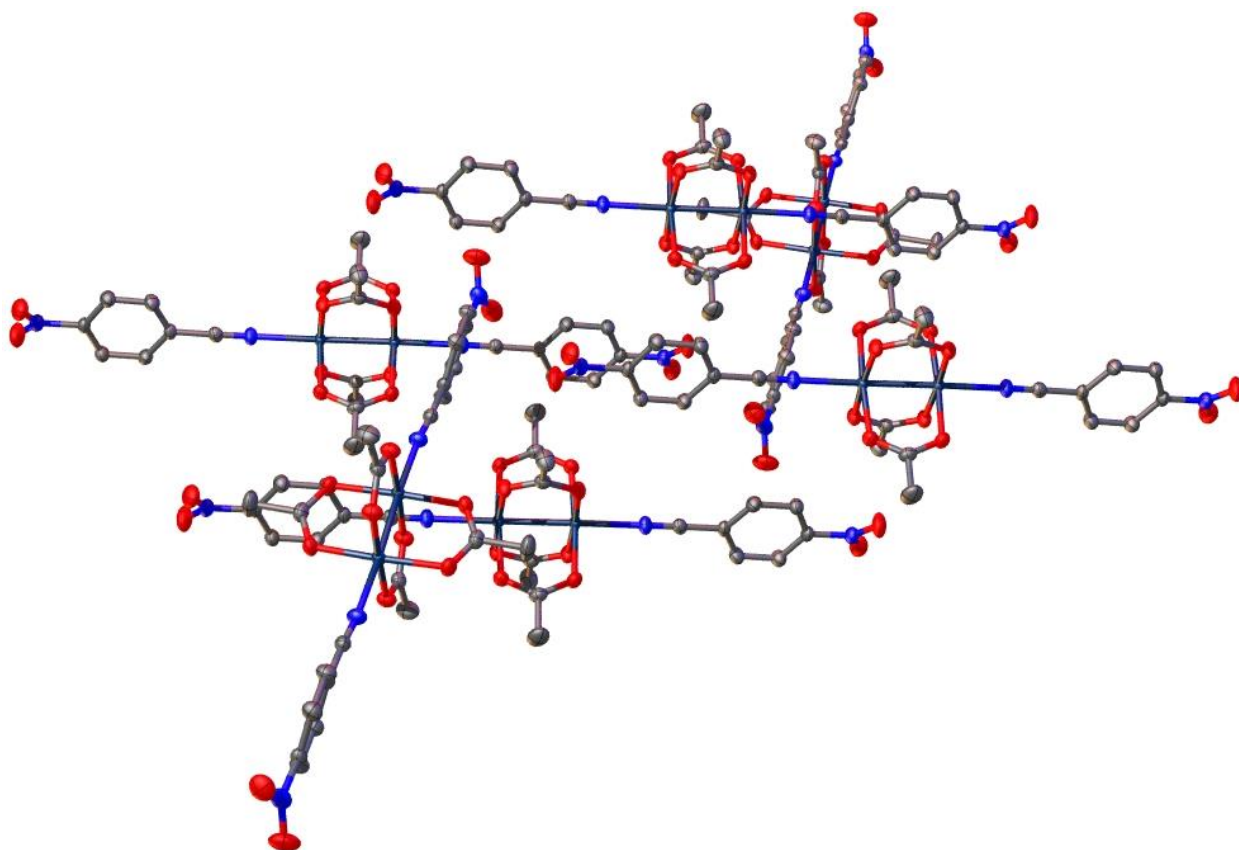
Figure 13: Packing diagram of 4-nitrobenzonitrile adduct.

3.1.2 The 4-aminobenzonitrile Adduct of Rh$_2$(OAc)$_4$

The [Rh$_2$(COOCH$_3$)$_4$]·2NCC$_6$H$_4$NH$_2$ crystal was a red platelet having approximate

dimensions of 0.290 x 0.280 x 0.140 mm mounted on a mitogen loop. The lattice parameters

measured for the crystal's unit cell determined that the [Rh$_2$(COOCH$_3$)$_4$]·2NCC$_6$H$_4$NH$_2$ crystal

system was primitive and orthorhombic. For Z=4 and formula weight equaling 678.26 g/mol, the

calculated density was 1.735 g/cm^3. A total of 540 oscillation images were collected.

Table 4: Crystal data for [Rh$_2$(COOCH$_3$)$_4$]·2NCC$_6$H$_4$NH$_2$.	
Empirical Formula	C$_{22}$H$_{24}$N$_4$O$_8$Rh$_2$
Formula Weight	678.26
Crystal Dimensions	0.290 x 0.280 x 0.140 mm
Crystal System	Orthorhombic
Lattice Type	Primitive
Lattice Parameters	a = 23.266(2) Å b = 11.639(1) Å c = 9.5862(9) Å V = 2595.9(5) Å^3
Space Group	Pbca (#61)
Residuals: R1 (I>2.00σ(I))	0.0262
Residuals: R (All reflections)	0.0386
Residuals: wR2 (All reflections)	0.0666
Goodness of Fit Indicator	0.954
Max Shift/Error in Final Cycle	0.002
Maximum peak in Final Diff. Map	0.49 e$^-$/Å^3
Minimum peak in Final Diff. Map	-0.29 e$^-$/Å^3

In Figure 14, a TEP of the 4-aminobenzonitrile adduct is shown. This TEP was created in

CrystalStructure, a software package (created by Rigaku) and can be called an Oak Ridge

Thermal Ellipsoid Plot (ORTEP), for the Oak Ridge National Laboratory. There is a slight bend

in the Rh1-N1-C5 bond angle. There is also a slight twist in the phenyl ring, meaning that is not

in either plain created by opposing acetate equatorial ligands. In addition, the hydrogens attached

to the N2 atom on the phenyl ring are slightly bent, likely due to the lone pair of electrons on the

nitrogen atom. This bending also lends itself to hydrogen bonding to the acetate ligands in

adjacent complexes, as can be seen in the packing diagram in Figure 15. Each complex

participates in four hydrogen bonds: two are found on the acetate ligands in which O3 and O3'

participates, and two in which a hydrogen on N2 participates. The distance of all of the close

contacts is 2.127 Å.
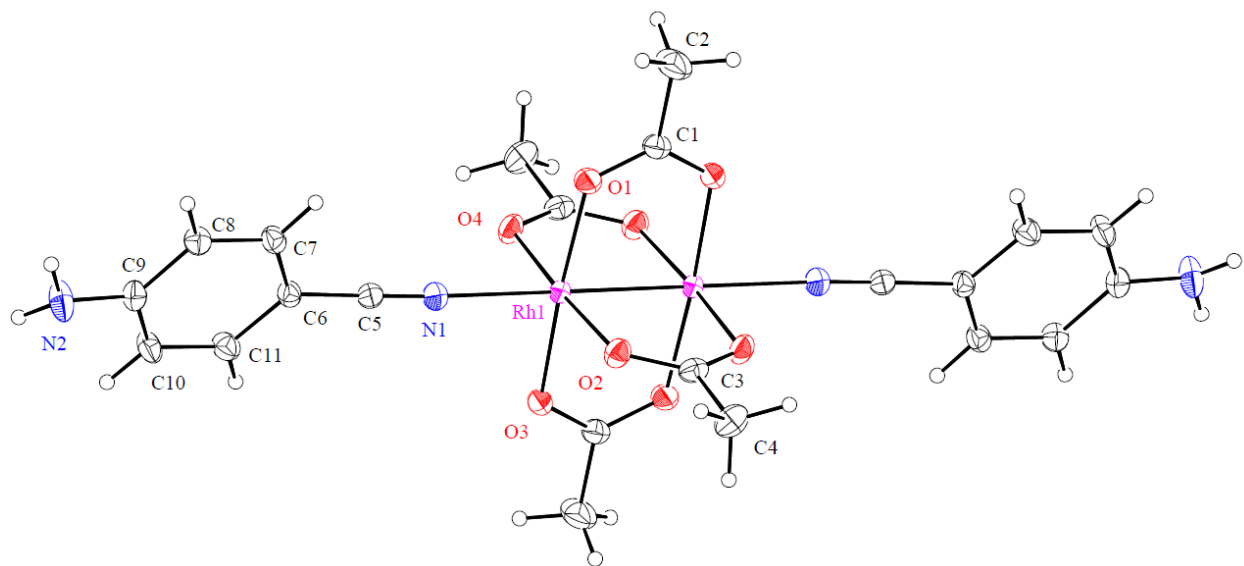
Figure 14: ORTEP of 4-aminobenzonitrile adduct.
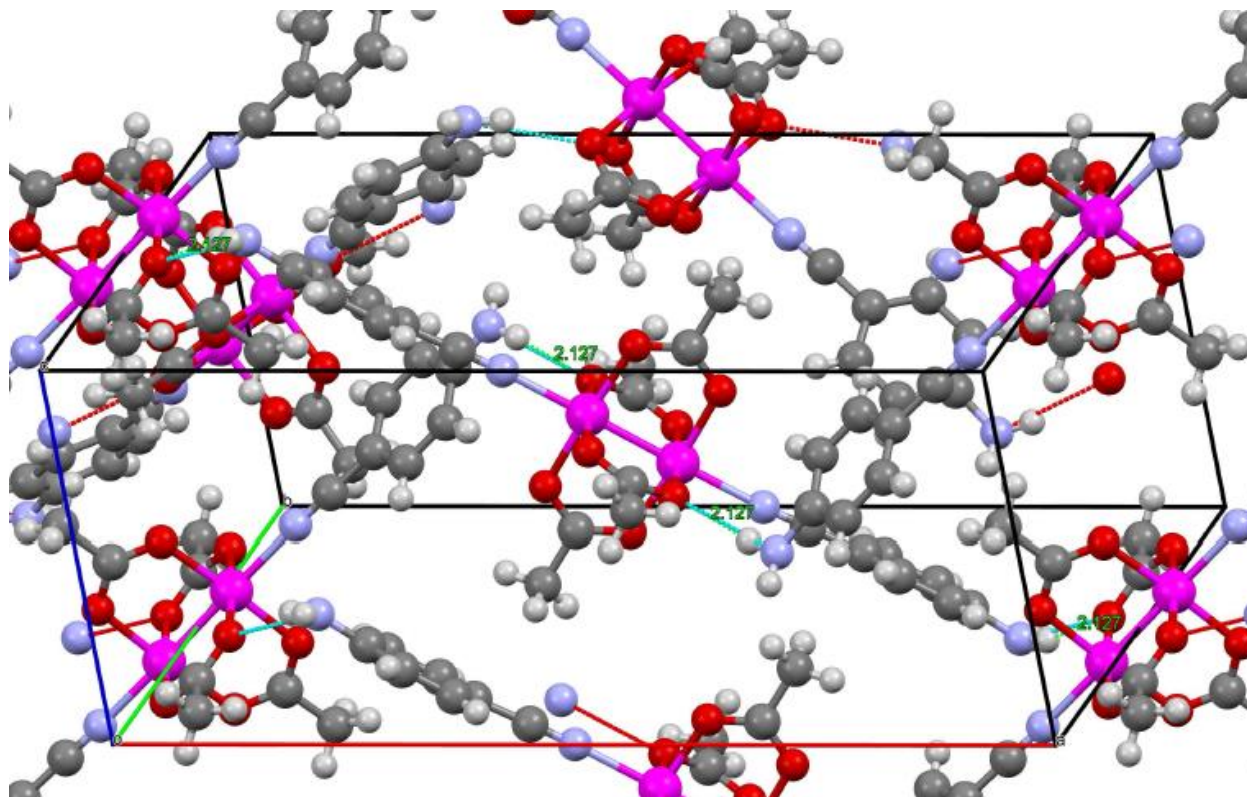
Figure 15: Packing diagram of 4-aminobenzonitrile adduct.

3.1.3 The 4-(dimethylamino)benzonitrile Adduct of $Rh_2(OAc)_4$

The $[Rh_2(COOCH_3)_4] \cdot 2NCC_6H_4N(CH_3)_2$ crystal was a red prism having approximate

dimensions of 0.200 x 0.150 x 0.120 mm mounted on a mitogen loop. The lattice parameters

measured for the crystal's unit cell determined that the $[Rh_2(COOCH_3)_4] \cdot 2NCC_6H_4N(CH_3)_2$

crystal system was primitive and monoclinic. For Z=2 and formula weight equaling 734.37

g/mol, the calculated density was 1.681 g/cm^3. A total of 540 oscillation images were collected.

Table 5: Crystal data for $[Rh_2(COOCH_3)_4] \cdot 2NCC_6H_4N(CH_3)_2$.	
Empirical Formula	$C_{26}H_{32}N_4O_8Rh_2$
Formula Weight	734.37
Crystal Dimensions	0.200 x 0.150 x 0.120 mm
Crystal System	Monoclinic
Lattice Type	Primitive
Lattice Parameters	a = 11.976(2) Å b = 8.054(2) Å c = 15.045(2) Å

	$\beta = 91.770(7)°$
	$V = 1450.4(4)$ Å^3
Space Group	P2$_1$/c (#14)
Residuals: R1 (I>2.00σ(I))	0.0326
Residuals: R (All reflections)	0.0411
Residuals: wR2 (All reflections)	0.1141
Goodness of Fit Indicator	0.902
Max Shift/Error in Final Cycle	0.013
Maximum peak in Final Diff. Map	0.52 e$^-$/Å^3
Minimum peak in Final Diff. Map	-0.78 e$^-$/Å^3

In Figure 16, an ORTEP of the 4-(dimethylamino)benzonitrile adduct is shown. There is a distinct bend in the Rh1-N1-C5 bond angle. Also, the bridging acetate ligands on the dirhodium(II) core are not perpendicular to one another. The reason for this can be seen in the packing diagram in Figure 17. The oxygen atoms of the acetate ligands participate in two types of dipole-dipole interactions. In the first type, O1 interacts with a hydrogen on C4 at a distance of 2.594 Å. In the second, O2 interacts with hydrogens on both C12 and C13 at a distance of 2.704 and 2.677 Å, respectively.
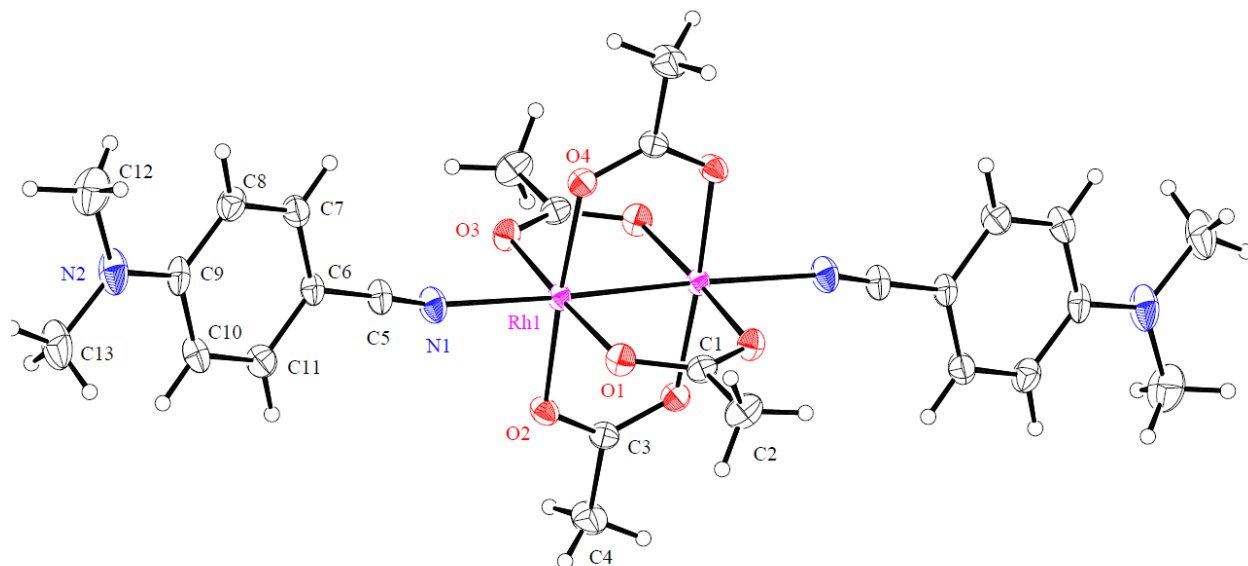
Figure 16: ORTEP of 4-(dimethylamino)benzonitrile adduct.
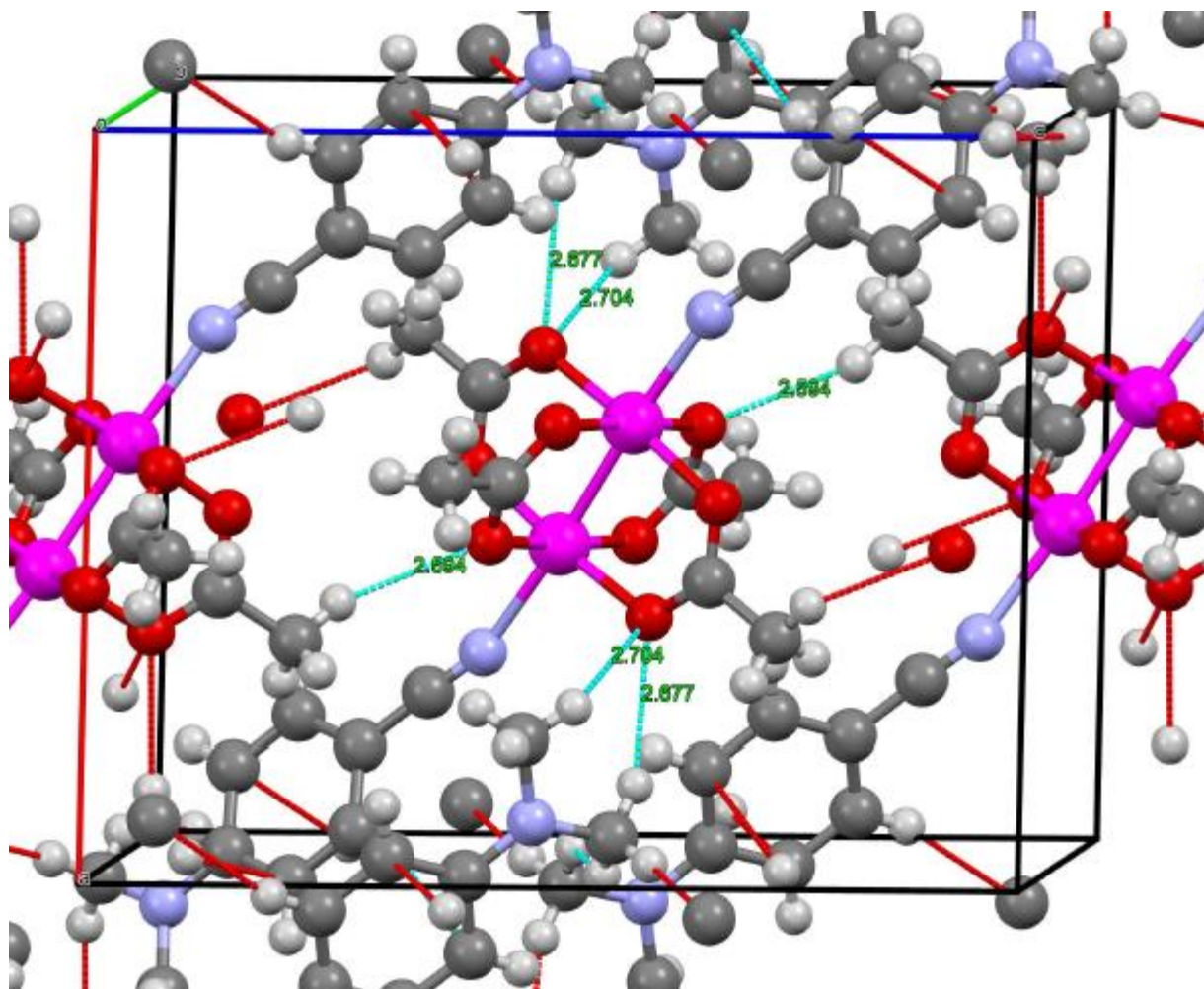
Figure 17: Packing diagram of 4-(dimethylamino)benzonitrile adduct.

3.1.4 The 3,5-dinitrobenzonitrile Adduct of Rh₂(OAc)₄

The $[Rh_2(COOCH_3)_4] \cdot 2NCOCH_2CH_3C_6H_3(NO_2)_2$ crystal was a red platelet having

approximate dimensions of 0.330 x 0.270 x 0.060 mm mounted on a mitogen loop. The lattice

parameters measured for the crystal's unit cell determined that the

$[Rh_2(COOCH_3)_4] \cdot 2NCOCH_2CH_3C_6H_3(NO_2)_2$ crystal system was monoclinic and primitive. For

Z=2 and formula weight equaling 828.23 g/mol, the calculated density was 1.633 g/cm³. A total

of 540 oscillation images were collected.

Table 6: Crystal data for [Rh$_2$(COOCH$_3$)$_4$]·2NCOCH$_2$CH$_3$C$_6$H$_3$(NO$_2$)$_2$.	
Empirical Formula	C$_{26}$H$_{28}$N$_6$O$_{18}$Rh$_2$
Formula Weight	828.23 g/mol
Crystal Dimensions	0.330 x 0.270 x 0.060 mm
Crystal System	Monoclinic
Lattice Type	Primitive
Lattice Parameters	a = 11.52150 Å b = 10.63880 Å c = 14.08500 Å β = 102.75300º V = 1683.87728 Å^3
Space Group	P2$_1$/n (#14)
Residuals: R1 (I>2.00σ(I))	0.0416
Residuals: R (All reflections)	0.0551
Residuals: wR2 (All reflections)	0.1428
Goodness of Fit Indicator	1.074
Max Shift/Error in Final Cycle	0.022
Maximum peak in Final Diff. Map	1.04 e$^-$/Å^3
Minimum peak in Final Diff. Map	-1.30 e$^-$/Å^3

Figure 18 shows an TEP of the 3,5-dinitrobenzonitrile adduct. This TEP was created in Mercury, a software package used to model crystal structures. The structure depicted here is quite different from what was expected, certainly different from the structures heretofore presented. C5 has reacted with an oxygen atom, O9, on an ethanol molecule. As a consequence of this, the C5-N1 triple bond (the nitrile) has lost electron density because of this reaction, which makes this bond longer (see Section 3.1.5). It can be said that the carbon atom, C5, has rehybridized from *sp* to *sp^2* hybridization. The *sp* hybridization gives the carbon atom a linear bonding geometry, while *sp^2* hybridization gives the carbon atom a planar bonding geometry, because the carbon atom here is bonded to a carbon, nitrogen, and oxygen atom, C6, N1, and O9, respectively. This structure, while unexpected, suggests that the Rh1-N1 bond has made C5 more reactive, perhaps by taking electron density away from the atom, allowing electron density from the oxygen atom to form a bond.
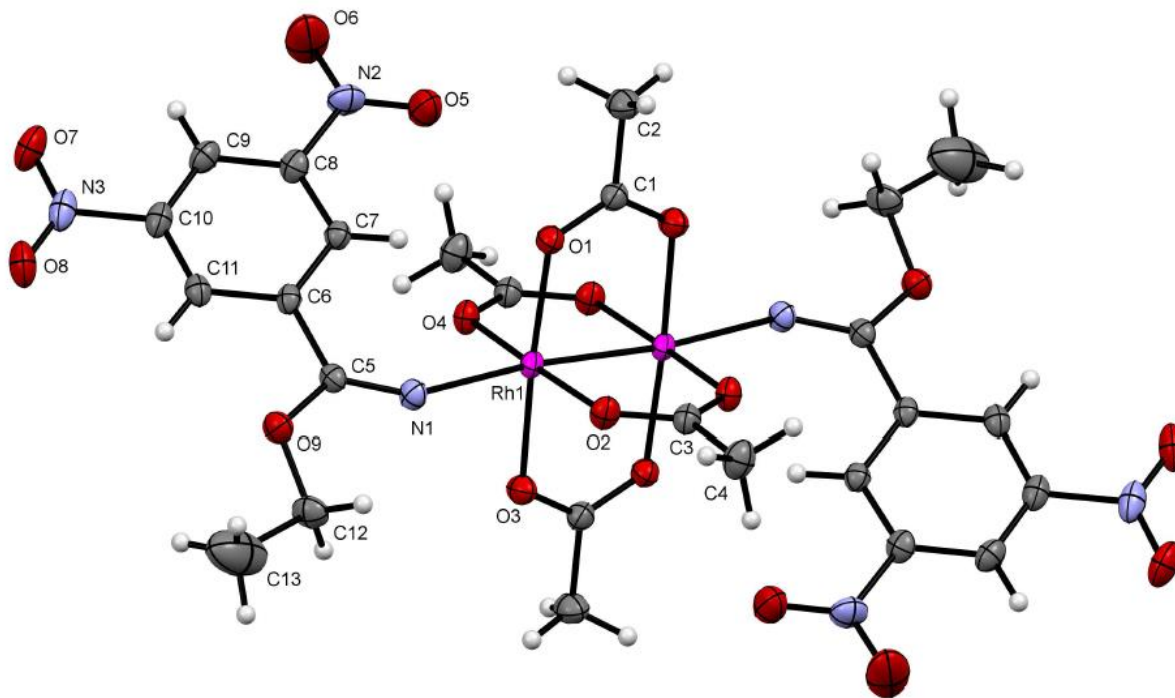
Figure 18: TEP of 3,5-dinitrobenzonitrile adduct.

The type reaction seen here, while previously unobserved for this catalyst, has been recorded in the literature.[19] The nitrile group is strongly polarized, giving the carbon atom a slight positive charge. This allows nucleophiles, atoms or molecules with a negative charge or lone pair of electrons, to interact with the nitrile group, yielding an sp^2 hybridized imine ion, shown in Figure 19. The two nitro groups on this specific benzonitrile in the *ortho-* position to the nitrile are strongly electron withdrawing, creating an even stronger positive charge on the nitrile carbon. This would give a nucleophile a better environment to react with the nitrile. Here because an ethanol molecule reacted with the nitrile, a systematic name for the reaction is nitrile alcoholysis. It can also be called the Pinner reaction for the German chemist Adolf Pinner, because of his work in the elucidation of the nature of this reaction and the detailed study of these compounds in 1892.[19,20] Traditionally the Pinner synthesis is carried out in an acid catalyst,

such as hydrochloric acid (in this case, the rhodium acetate functions as a Lewis acid). Also, the synthesis is normally carried out at 0 °C, otherwise the imidate salt would decompose into an amide, making the reaction observed in this study even more extraordinary. In this reaction, $Rh_2(OAc)_4$ has apparently stabilized the transient species to prevent amide formation. Thus, the resulting product can be used to understand the mechanism of the Pinner reaction.
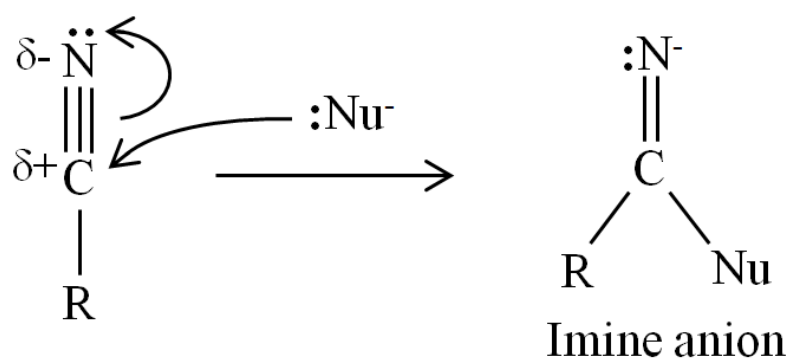
Figure 19: Formation of imine anion.

Figure 20 shows the packing diagram for the 3,5-dinitrobenzonitrile adduct. There are several dipole-dipole interactions stabilizing the crystal structure, all stemming from the two nitro functional groups. O5 interacts with a hydrogen atom on C13 at a distance of 2.535 Å. N2 interacts with this same atom at a distance of 2.705 Å. O6 interacts with a hydrogen atom on C9 at a distance of 2.564 Å. O7 interacts with hydrogen atoms on C12 and C4 at distances of 2.651 Å and 2.524 Å, respectively. Last, O8 interacts with a hydrogen atom on C2 at a distance of 2.591 Å. Due to the interactions from the nitro oxygen atoms on the carbon atoms' hydrogens in the ethanol molecule, it is also possible that the position of the nitro groups in the crystal lattice helped hold the ethanol molecule in place in order for a reaction to occur.
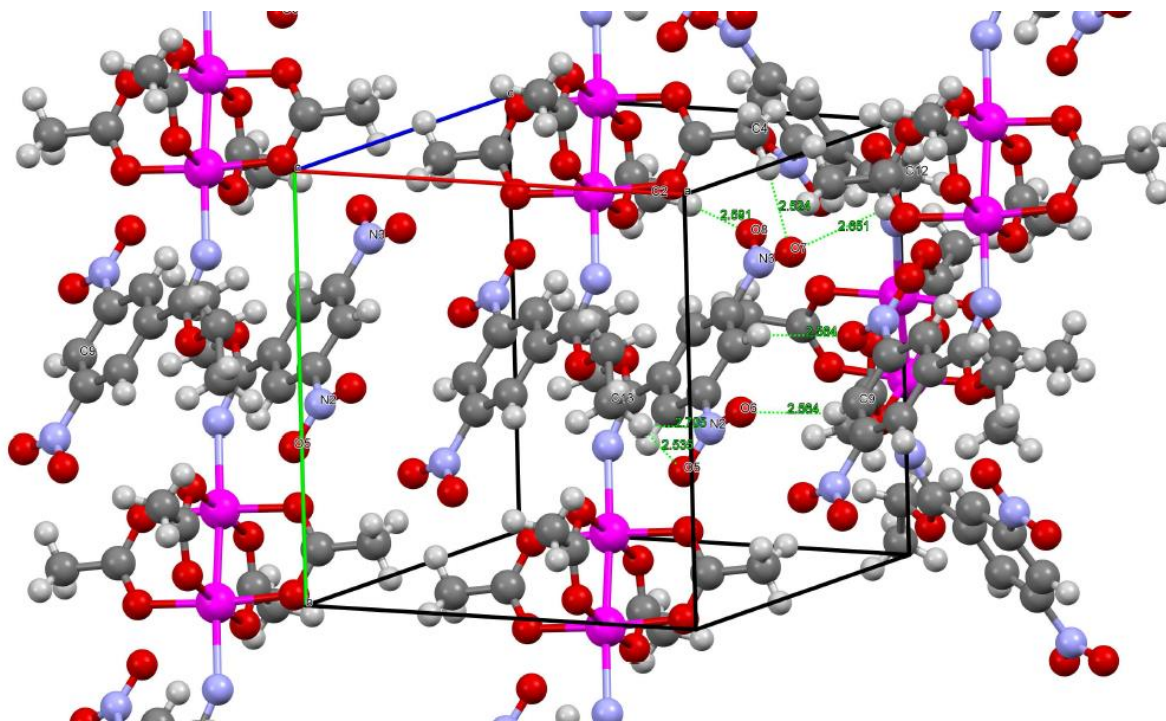
Figure 20: Parking diagram of the 3,5-dinitrobenzonitrile adduct.

What would the Pinner reaction look like for the 3,5-dinitrobenzonitrile adduct specifically? First, one of the lone pairs of electrons on the oxygen atom of the ethanol molecule would attack the carbon atom of the nitrile, forming a chemical bond. This means that the electrons used in one of the carbon to nitrogen triple bonds would be displaced onto the nitrogen atom. At this point, the oxygen atom would have a positive formal charge due to the fact that it has formed three bonds and the nitrogen atom would have a negative formal charge because of the extra pair of electrons.

This then could lead to two different results, as depicted in Figure 21. One is that the formal charges are maintained and a zwitterion, or a "hybrid" ion with both positive and negative charges, is formed. The second possibility is that the oxygen atom loses its hydrogen atom and a salt is formed with the hydrogen now attached to the nitrogen atom. For this option to occur, another nucleophile, such as water, must abstract the hydrogen atom in order to form the salt; the

hydrogen cannot leave on its own. In the crystal structure of this adduct, there was no additional

oxygen near the hydrogen atom, suggesting that salt formation did not occur. This makes the

zwitterion the more likely candidate. Because hydrogen atoms cannot be located by X-ray

crystallography and can only be calculated, another characterization method must be used such

as nuclear magnetic resonance (NMR) spectroscopy, in order to confirm the presence of this

hydrogen atom.
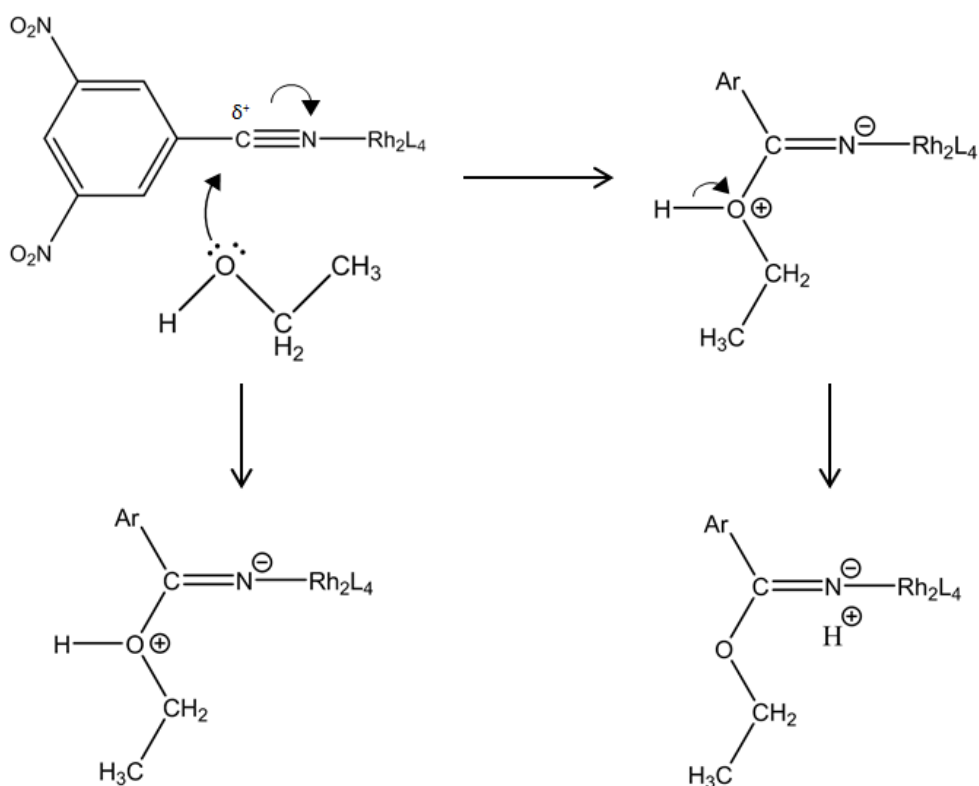
Figure 21: Proposed Pinner mechanism for the 3,5-dinitrobenzonitrile adduct.

3.1.5 Selected Bond Distances and Angles

Because the purpose of this research was to better understand the bonding between the

rhodium atom and axial ligands, this section will discuss bond distances and angles that are most

relevant to that end. In all four structures, the rhodium-rhodium bond distance was consistently

around 2.39-2.40 Å, showing that the dirhodium core is quite stable and is not influenced by

axial ligation. The rhodium-nitrogen and nitrogen-carbon bond distances are almost as

consistent, with the exception of the 3,5-dinitrobenzonitrile adduct, principally due to the ethanol

molecule that attached to the carbon.

The rhodium-rhodium-nitrogen and rhodium-nitrogen-carbon bond angles are not as

consistent as the bond distances, again with the 3,5-dinitrobenzonitrile adduct deviating from the

other three. The 4-aminobenzonitrile adduct has bond angles closest to linearity, which would be

expected if π-backbonding were to occur. The reason that true linearity is not observed in any of

the four adducts is likely due the intermolecular close contacts that keep the solid state together,

as evidenced most distinctly by the 3,5-dinitrobenzonitrile. For this reason, it can be ascertained

that if π-backbonding were to exist in any of these adducts, it would have to be stronger than the

intermolecular forces. Table 7 provides the bond distances and angles discussed above.

Table 7: Selected bond distances and angles.				
	4-nitrobenzo-nitrile adduct	4-aminobenzo-nitrile adduct	4-(dimethyl-amino)benzonitrile adduct	3,5-dinitro-benzonitrile adduct
Distances (Å)				
Rh-Rh	2.3926(4)	2.3914(3)	2.3911(4)	2.3965(5)
Rh-N	2.225(2)	2.228(2)	2.238(3)	2.286(3)
N-C	1.131(3)	1.144(4)	1.137(4)	1.273(5)
Angles (°)				
Rh-Rh-N	175.54(6)	179.02(6)	176.10(7)	173.80(9)
Rh-N-C	172.9(2)	177.0(2)	162.4(2)	146.2(3)

The bonding for the benzonitriles above can be compared to the phenyl isonitriles

published by the Eagle group.[15] In fact, the 4-(dimethylamino) functional group can be compared

directly, both anticipated to be quite electron withdrawing. This data is shown in Table 8. First

for the 4-(dimethylamino)-substituted adducts, the Rh-N bond is longer than the corresponding

Rh-C bond likely because nitrogen is a larger atom than carbon. The N-C bond is almost the

same in both structures at about 1.14 Å. The Rh-N-C and Rh-C-N bond angles both in the 160s,

possibly due to electron donating capability but more likely due to steric hindrance because the 4-(dimethylamino) substituent is quite bulky. In the isonitrile adducts the Rh-Rh bond is consistent throughout its series at around 2.42 Å.

Table 8: Selected bond distances and angles for isonitriles.[15]			
	4-(dimethylamino)-phenyl isonitrile adduct	Phenyl isonitrile adduct	Trifluoromethylphenyl isonitrile adduct
Distances (Å)			
Rh-Rh	2.4245(4)	2.4271(3)	2.4182(3)
Rh-C	2.148(4)	2.133(3)	2.122(3)
C-N	1.139(5)	1.153(4)	1.141(5)
Angles (°)			
Rh-C-N	166.8(4)	158.7(2)	155.4(3)

3.2 IR Spectroscopy

Infrared spectroscopy was used here to assist in understanding the type of bonds that occur in the novel rhodium acetate adducts, particularly the rhodium to nitrogen bond in the axial site. If π-backbonding were to occur, the carbon to nitrogen bond in the nitrile should become weaker and be lower in energy. The stretching frequency therefore should decrease because energy is directly proportional to it.

$$E = h\nu = \frac{hc}{\lambda} = hc\bar{\nu}$$

All IR data was taken in the solid phase, using attenuated total reflectance (ATR). Spectra for the following four novel rhodium acetate adducts were successfully obtained: the adducts with 4-nitrobenzonitrile, 4-aminobenzonitrile, 4-(dimethylamino)benzonitrile and 3,5-dinitrobenzonitrile. Spectra for each unreacted benzonitrile were also obtained. The spectrum for each adduct is followed by its corresponding benzonitrile, given in Figures 22-29 and selected wavenumbers are given in Tables 9-16 for clarity.

For all of the adducts' spectra, a distinct pattern appears in what is considered the nitrile absorbing region. There are two distinct peaks at 2378.23 and 2310.72 cm^{-1}, separated by a sharp peak in the middle. In figures 24 and 26, there is a peak to the right of this pattern, at 2235.50 and 2223.92 cm^{-1}, respectively. In the unreacted benzonitriles' spectra, there are also two distinct peaks. One peak is consistent throughout: 2358.94 cm^{-1}. The second peak, however, is different for each benzonitrile. For both nitrobenzonitriles, the peak is at 2341.58 cm^{-1} and the peaks for 4-aminobenzonitrile and 4-(dimethylamino)benzonitrile are at 2331.94 and 2330.01 cm^{-1}, respectively.

The peak at 2378.23 cm^{-1} is higher in wavenumber than the corresponding unreacted peak, suggesting that the carbon to nitrogen bond in the nitrile has gained energy. This does not support the π-backbonding hypothesis in the axial ligation at the rhodium site. This may indicate predominantly σ-bonding for the rhodium to nitrogen bond in all of the adducts.
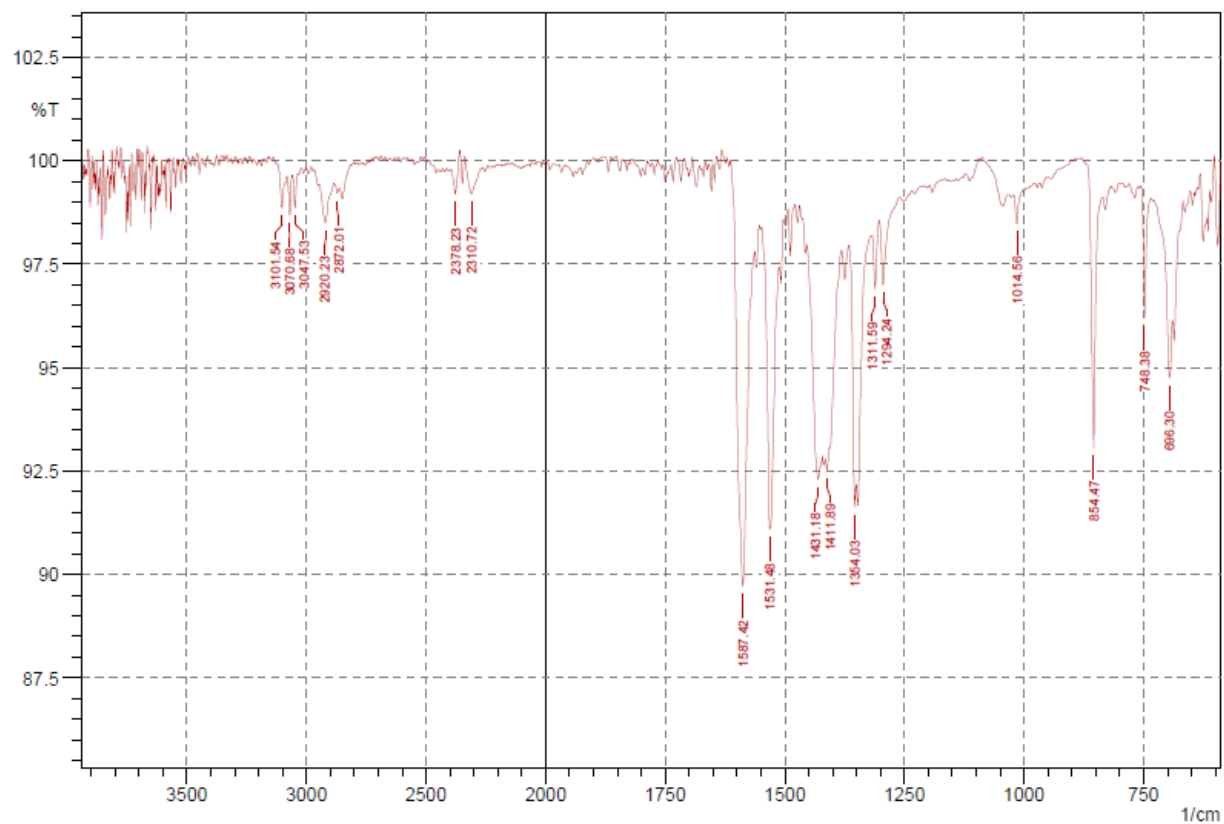
Figure 22: IR spectrum of the 4-nitrobenzonitrile adduct.

Table 9: Selected wavenumbers for the 4-nitrobenzonitrile adduct (cm^{-1}).
3101.54
3070.68
3047.53
2920.23
2378.23
2310.72
1587.42
1354.03
1014.56
854.47
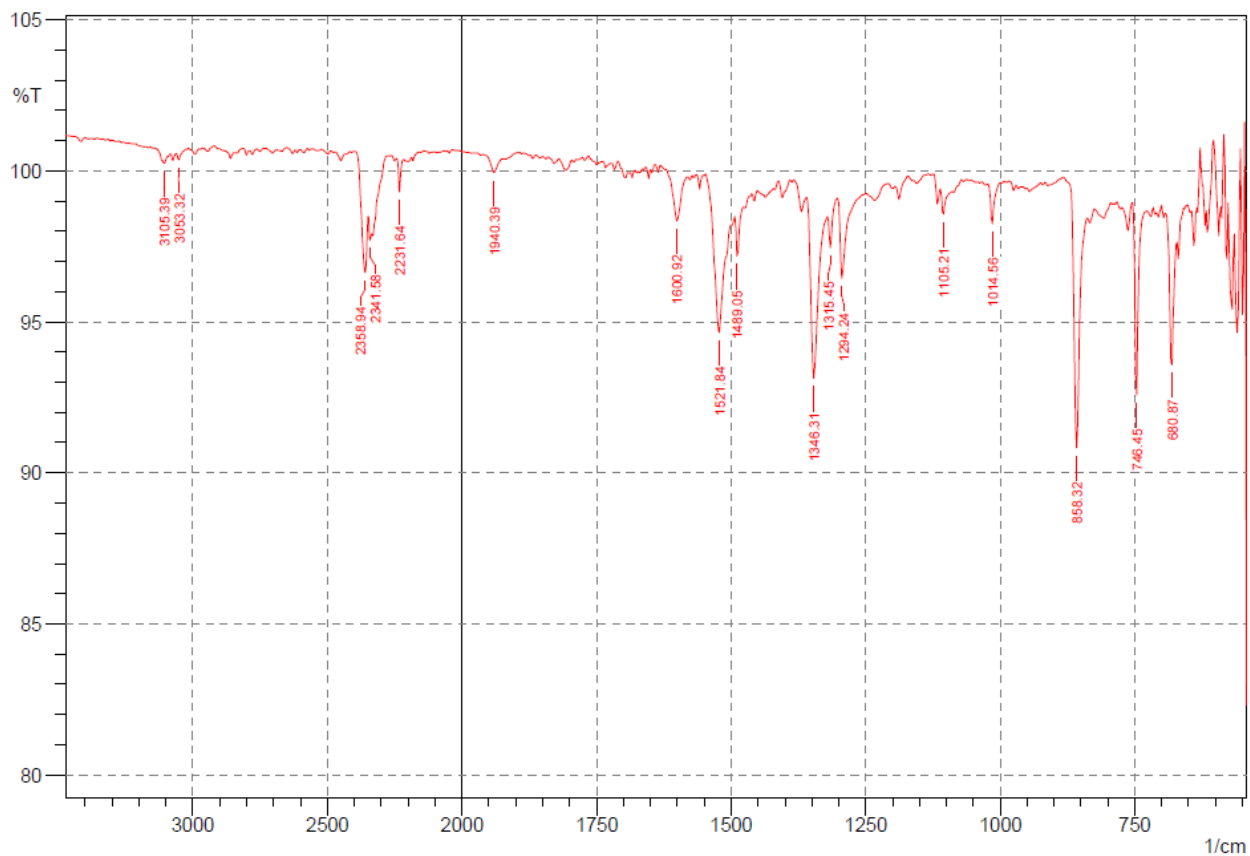
Figure 23: IR spectrum of 4-nitrobenzonitrile.

Table 10: Selected wavenumbers for 4-nitrobenzonitrile (cm^{-1}).
3105.39
3053.32
2358.94
2341.58
2231.64
1940.39
1600.92
1521.84
1346.31
858.32
746.45
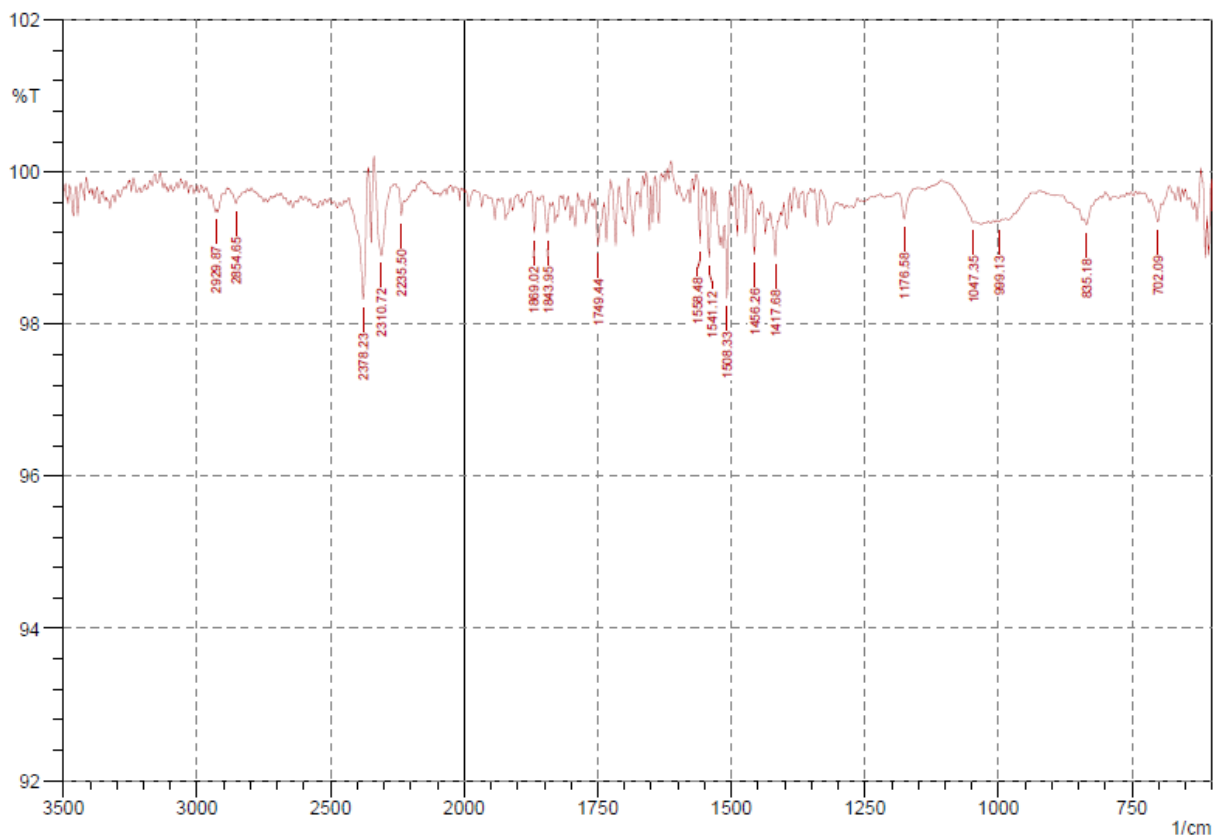
Figure 24: IR spectrum of the 4-aminobenzonitrile adduct.

Table 11: Selected wavenumbers for 4-aminobenzonitrile adduct (cm^{-1}).
2929.87
2854.65
2378.23
2310.72
2235.50
1869.02
1508.33
1176.58
1047.35
835.18
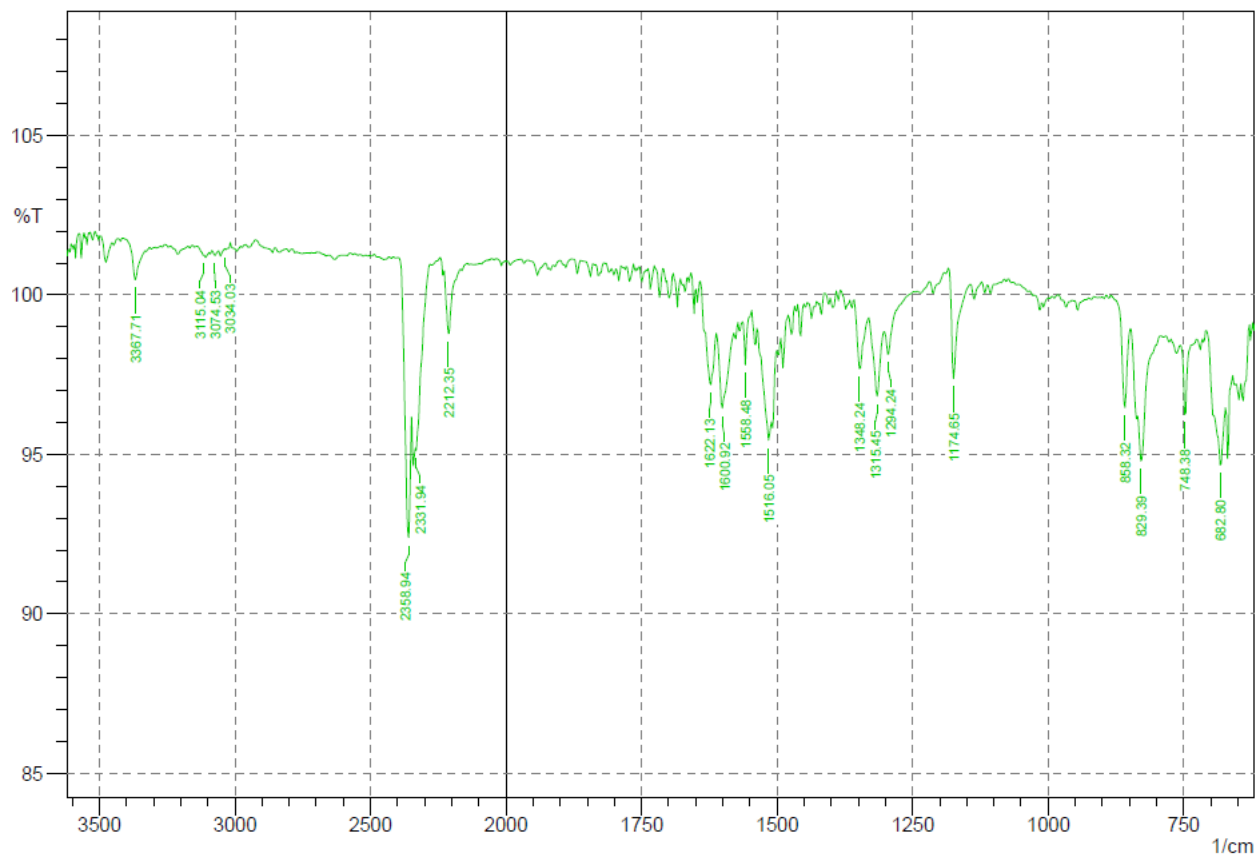
Figure 25: IR spectrum of 4-aminobenzonitrile.

Table 12: Selected wavenumbers for 4-aminobenzonitrile (cm^{-1}).
3367.71
3074.53
2358.94
2331.94
2212.35
1600.92
1516.05
1315.45
1174.65
829.39
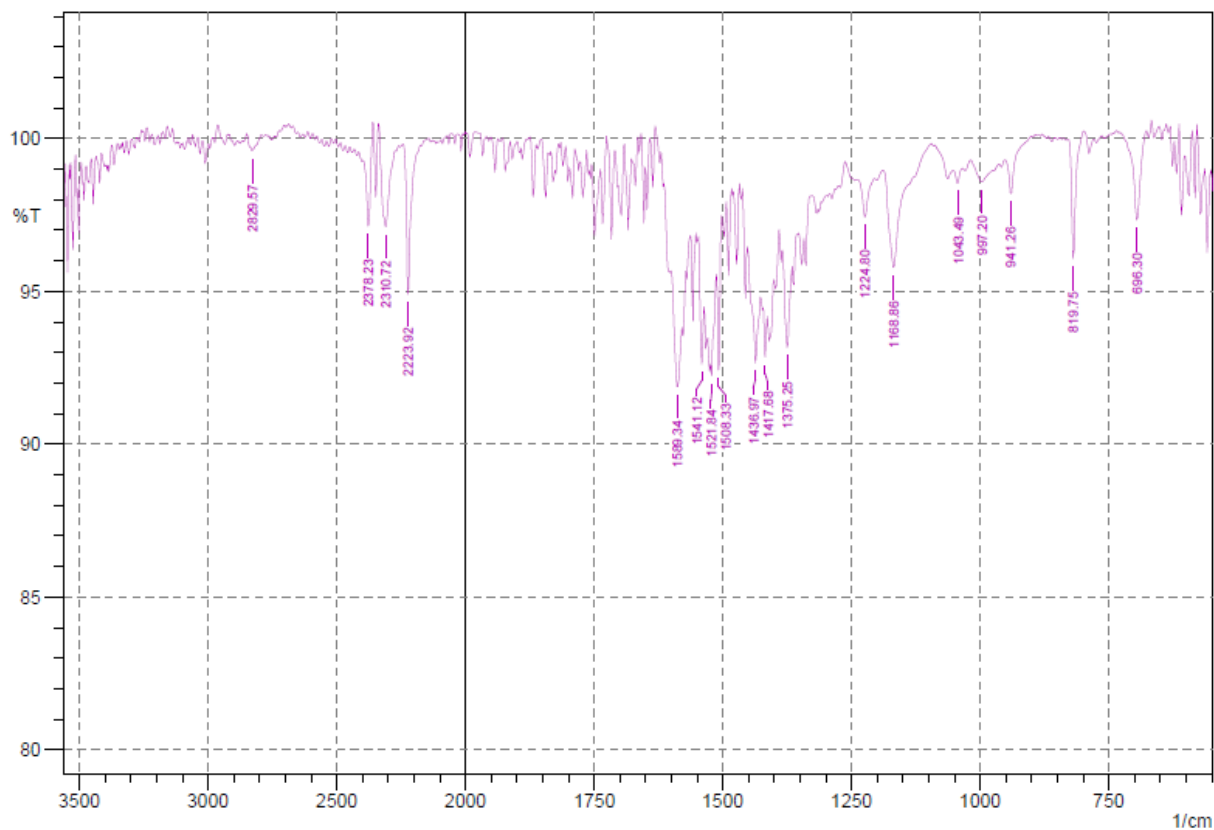
Figure 26: IR spectrum of the 4-(dimethylamino)benzonitrile adduct.

Table 13: Selected wavenumbers for the 4-(dimethylamino)benzonitrile adduct (cm^{-1}).
2829.57
2378.23
2310.72
2223.92
1589.34
1508.33
1168.86
1043.49
819.75
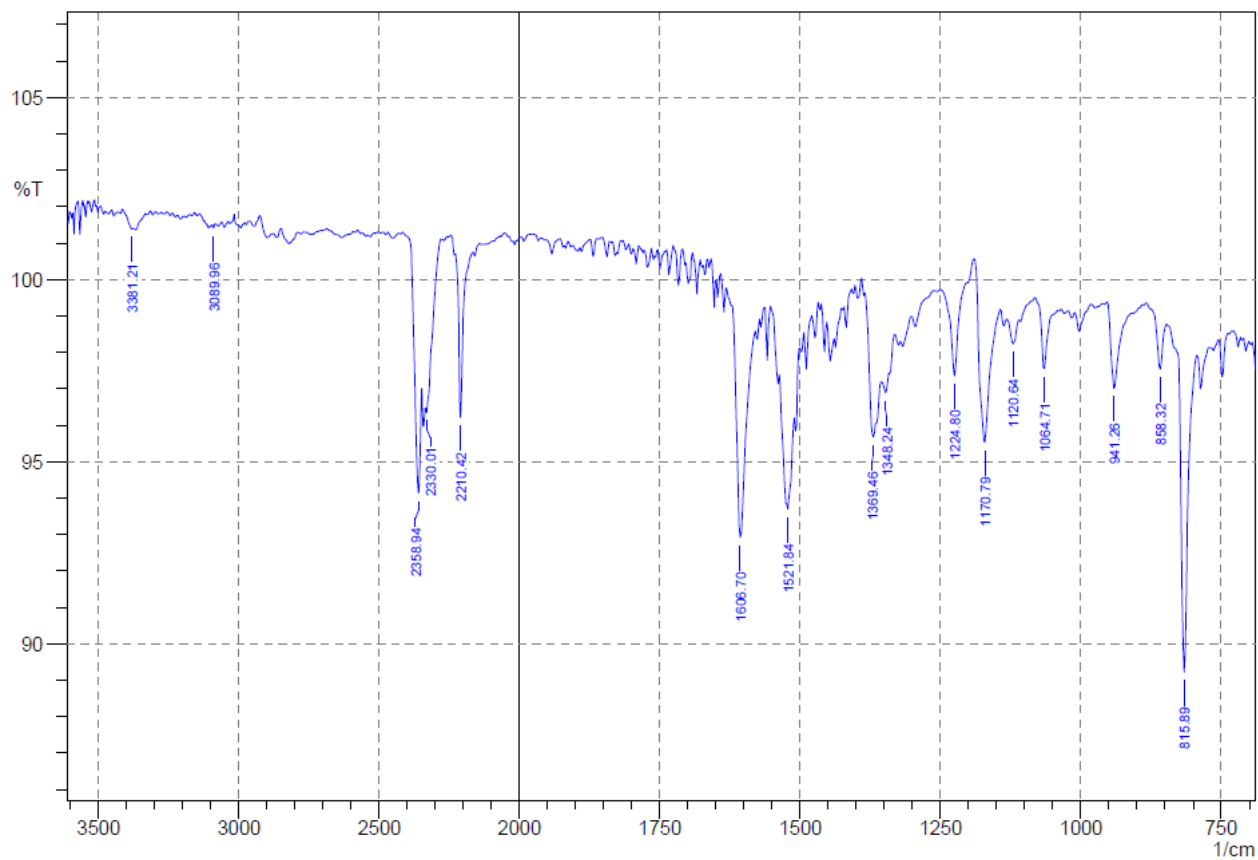
Figure 27: IR spectrum of 4-(dimethylamino)benzonitrile.

Table 14: Selected wavenumbers for 4-(dimethylamino)benzonitrile (cm^{-1}).
3381.21
2358.94
2330.01
2210.42
1606.70
1521.84
1170.79
815.89
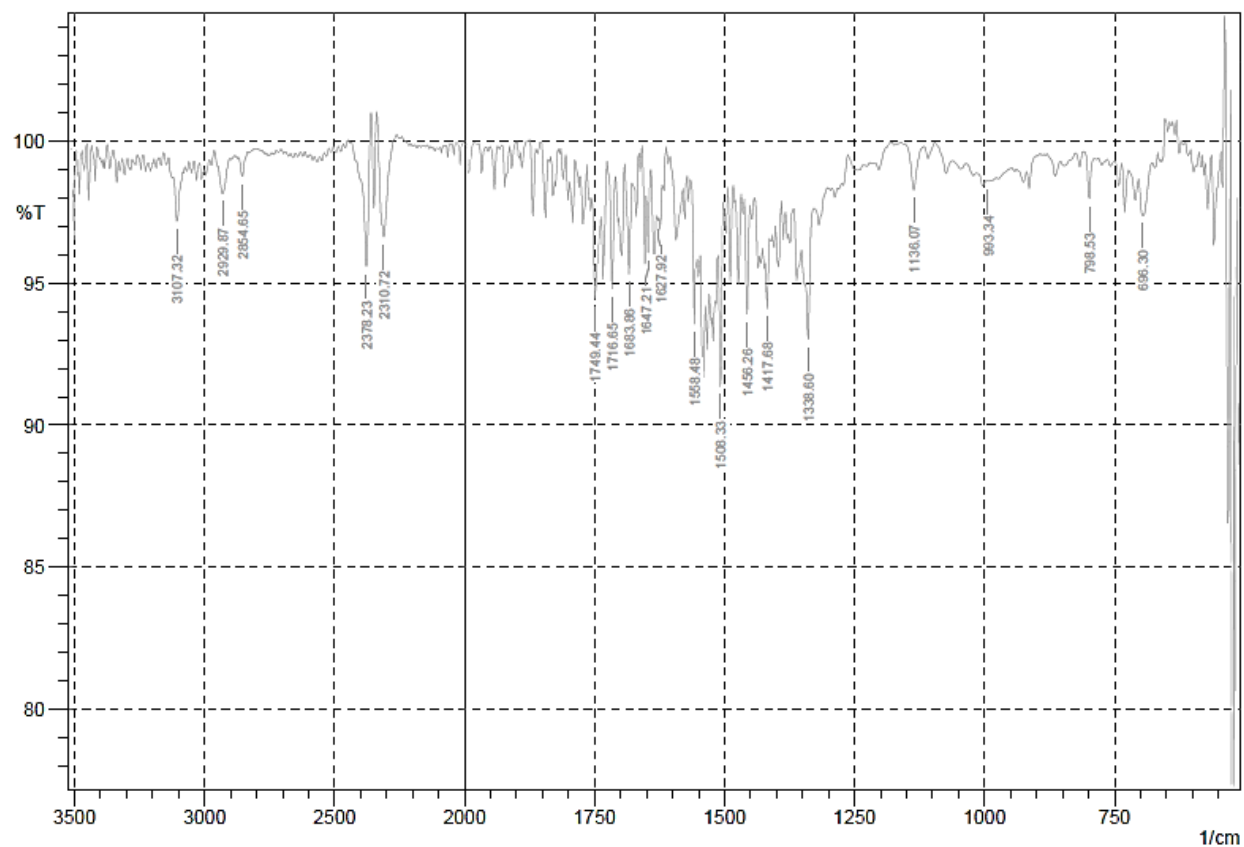
Figure 28: IR spectrum of the 3,5-dinitrobenzonitrile adduct.

Table 15: Selected wavenumbers for the 3,5-dinitrobenzonitrile adduct (cm^{-1}).
3107.32
2929.87
2854.65
2378.23
2310.72
1749.44
1508.33
1417.68
1338.60
1136.07
993.34
798.53
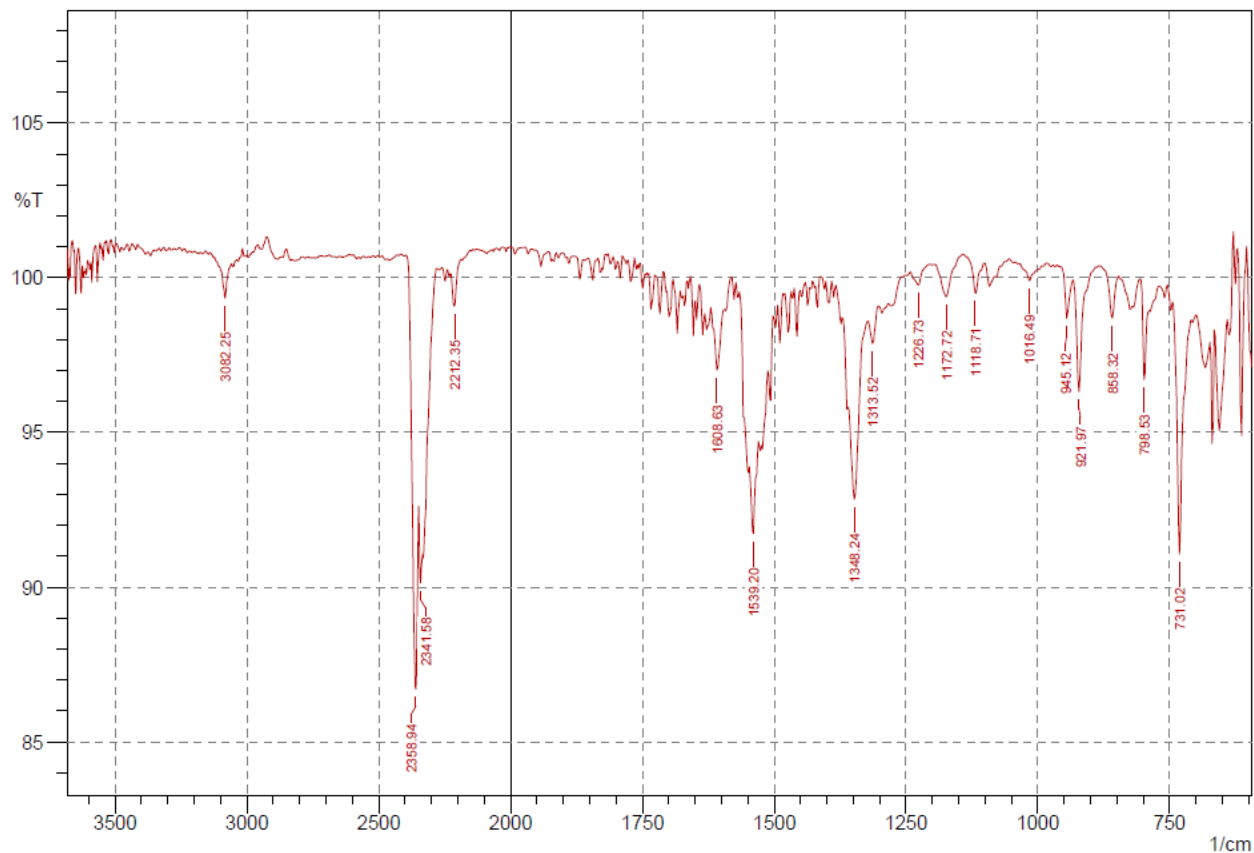
Figure 29: IR spectrum of 3,5-dinitrobenzonitrile.

Table 16: Selected wavenumbers for 3,5-dinitrobenzonitrile (cm^{-1}).
3082.25
2358.94
2341.58
2212.35
1539.20
1348.24
921.97
798.53
731.02

3.3 NMR Spectroscopy

Nuclear Magnetic Resonance (NMR) spectroscopy is an excellent technique that allows

for the detection of uniquely positioned atoms in a compound, granted that these atoms have a

non-integer spin value. NMR spectroscopy is also solution based, while the X-ray

crystallography and IR spectroscopy techniques discussed above analyzed the novel compounds

48

in the solid state. NMR spectroscopy therefore gives insight about these compounds in a different chemical environment, lending to the possibility to structural phenomena not available in the crystalline state. This technique also lends itself to the discussion of purity of the compounds, for example, whether or not there is a significant amount of unreacted benzonitrile present in the solution.

The solvent used in this study was deuterated chloroform ($CDCl_3$) and three of the four adducts were soluble in the chloroform and therefore able to produce ^{1}H NMR spectra: the 4-nitrobenzonitrile, 4-(dimethylamino)benzonitrile, and 3,5-dinitrobenzonitrile adducts. The 4-aminobenzonitrile adduct was insoluble in $CDCl_3$. At the time of this paper, no further attempts have been made to ascertain a spectrum for this adduct. NMR spectra for each of the uncomplexed ligands are available in the literature and will be used for the discussion that follows.[21-23] NMR spectra for the adducts were used here only to determine the hydrogen atom's chemical environment. While integration of the peaks was attempted, they were not proportional to each other. Integration data was lost due to the temporary breakdown of the NMR instrument. When the repairs were complete the original data was erased.

Note: for this discussion, the term deshielded describes a peak that has been shifted downfield, or to the left, of the NMR spectrum and the term shielded describes a peak that has been shifted upfield, or to the right, of the NMR spectrum.

Figures 30 and 31 show the 4-nitrobenzonitrile adduct and unreacted 4-nitrobenzonitrile, respectively. We would expect to see three peaks on the adduct: one from the methyl group from the equatorial acetate ligands on the rhodium complex, and two from the phenyl ring of the axial ligand. These peaks are assigned a, b, and c, and are shown in Figure 30. In total, there are five peaks, the three just mentioned as well as one from the chloroform at δ 7.2548 and one from

water at δ 1.6746. The methyl peak, a, is thus located at δ 2.0290. When Figures 30 and 31 are compared, there are two sharp peaks at approximately δ 8.35 and δ 7.85 in the unreacted 4-nitrobenzonitrile that correspond to the peaks at δ 8.45 and 8.1551, respectively, labeled b and c. This indicates that upon reaction, the phenyl peaks shifted downfield by δ 0.10, meaning they have been deshielded. Losing electron density supports evidence of reaction and σ-bonding from the nitrogen atom to the rhodium atom.
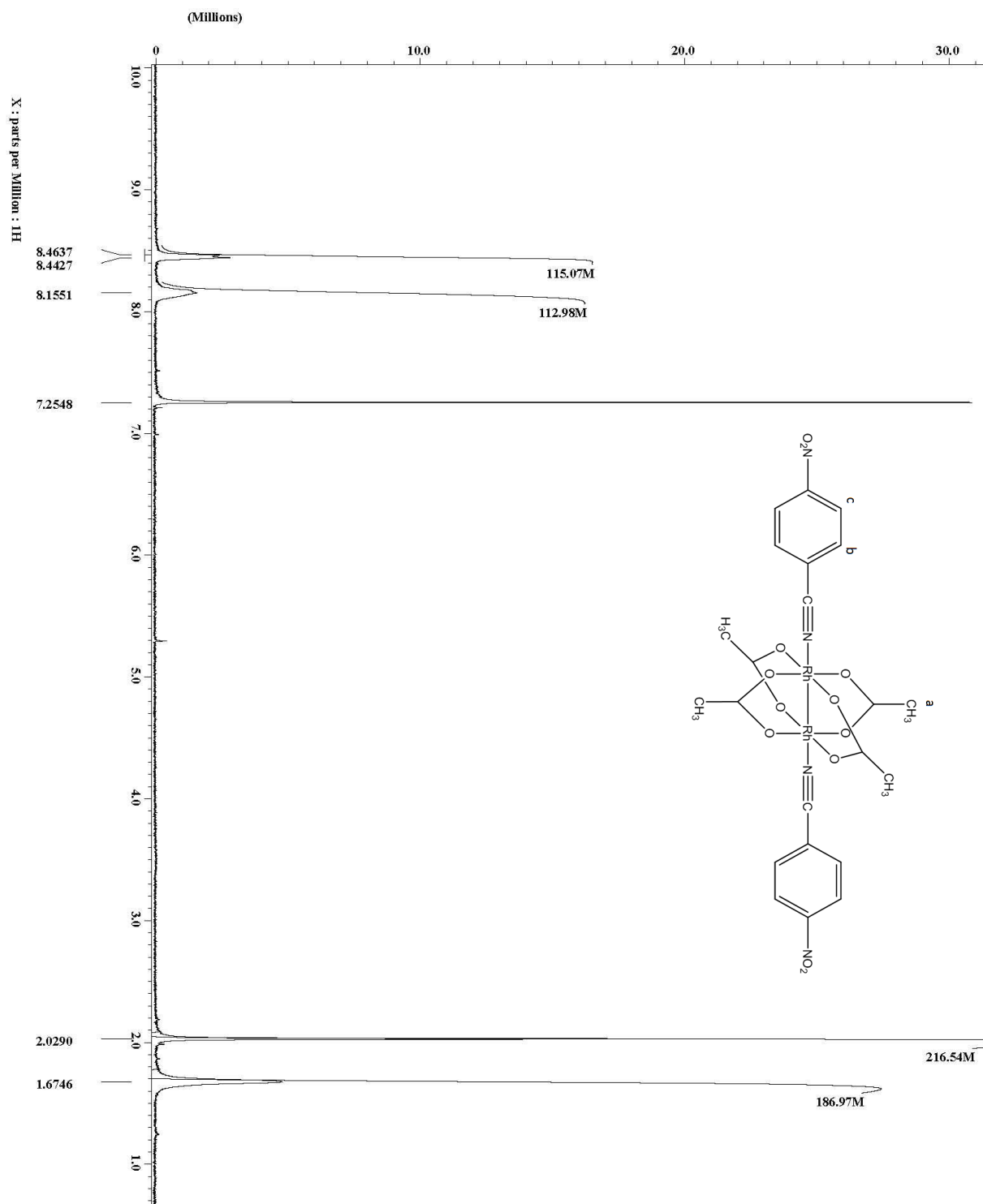
Figure 30: NMR spectrum of the 4-nitrobenzonitrile adduct.
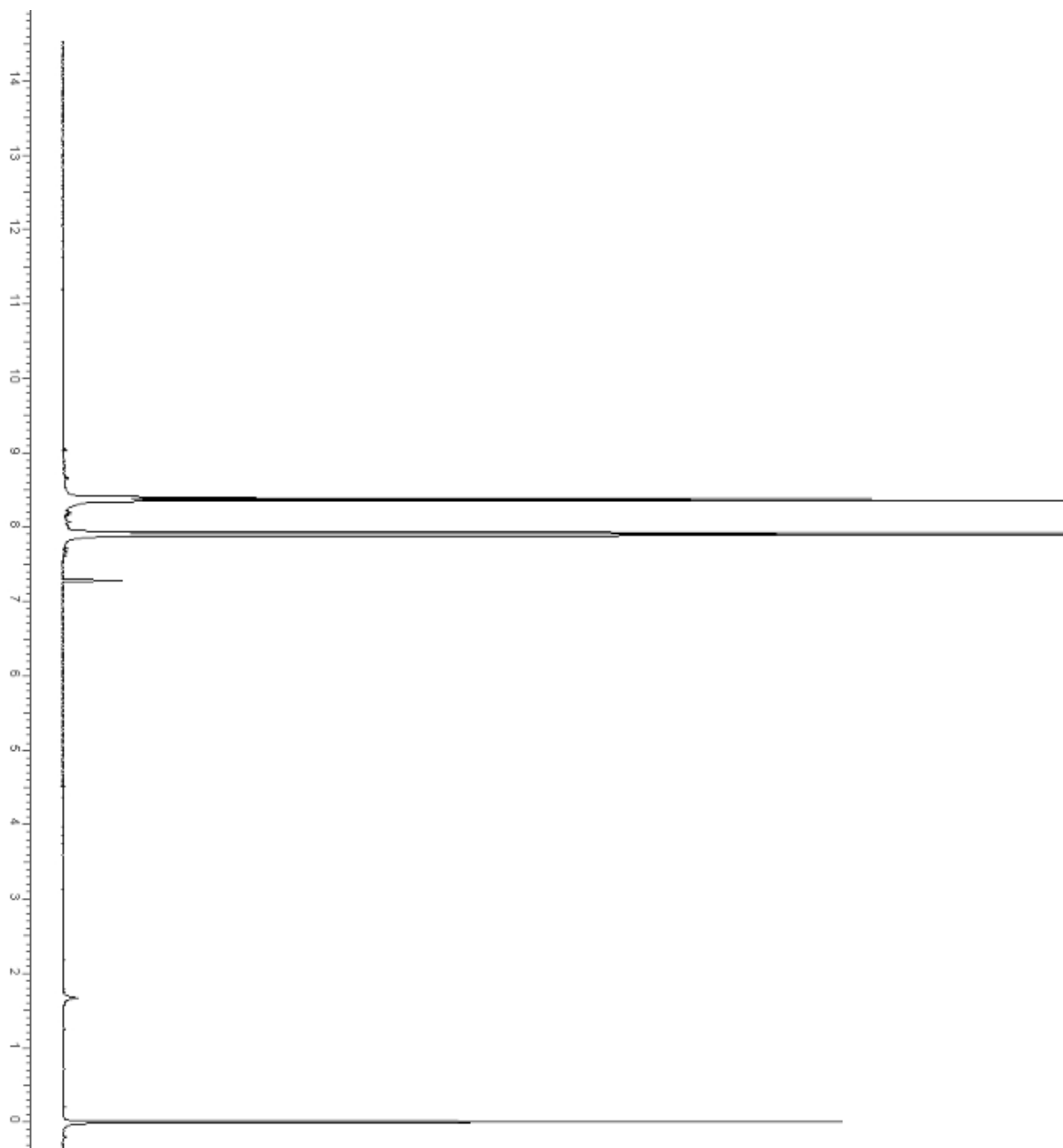
Figure 31: Literature NMR spectrum of 4-nitrobenzonitrile.[21]

Figures 32 and 33 show the 4-(dimethylamino)benzonitrile adduct and unreacted 4-

(dimethylamino)benzonitrile, respectively. We would expect to see four peaks on the adduct: one

from the methyl group from the equatorial ligands on the rhodium complex, two from the phenyl

ring of the axial ligand, and one from the methyl groups on the amine also on the axial ligand.

These peaks are assigned a, b, c, and d. In Figure 32 there are approximately seven peaks,

including the chloroform peak at δ 7.2548 and water at δ 1.5757. The methyl peak from the

acetate ligands, a, is thus located at δ 2.0015. When Figures 32 and 33 are compared, there are

three sharp peaks at approximately δ 7.4, δ 6.6, and δ 3.01 in the unreacted 4-

(dimethylamino)benzonitrile that correspond to the peaks at δ 7.75, δ 6.7951, and δ 3

respectively, labeled b, c and d. There are two peaks around δ 3: δ 3.0978 and δ 3.0053. This

indicates that there is some unreacted benzonitrile in the solution. This also indicates that upon

reaction, the phenyl and methyl peaks from the reacted benzonitrile shifted downfield by varying

degrees, meaning that the peaks on the phenyl ring were shifted downfield more than the methyl

peaks on the amine. This is reasonable because the phenyl electrons are in resonance with the

nitrile and the methyl electrons of the amine are not. Losing electron density supports evidence

of reaction and σ-bonding from the nitrogen atom to the rhodium atom.
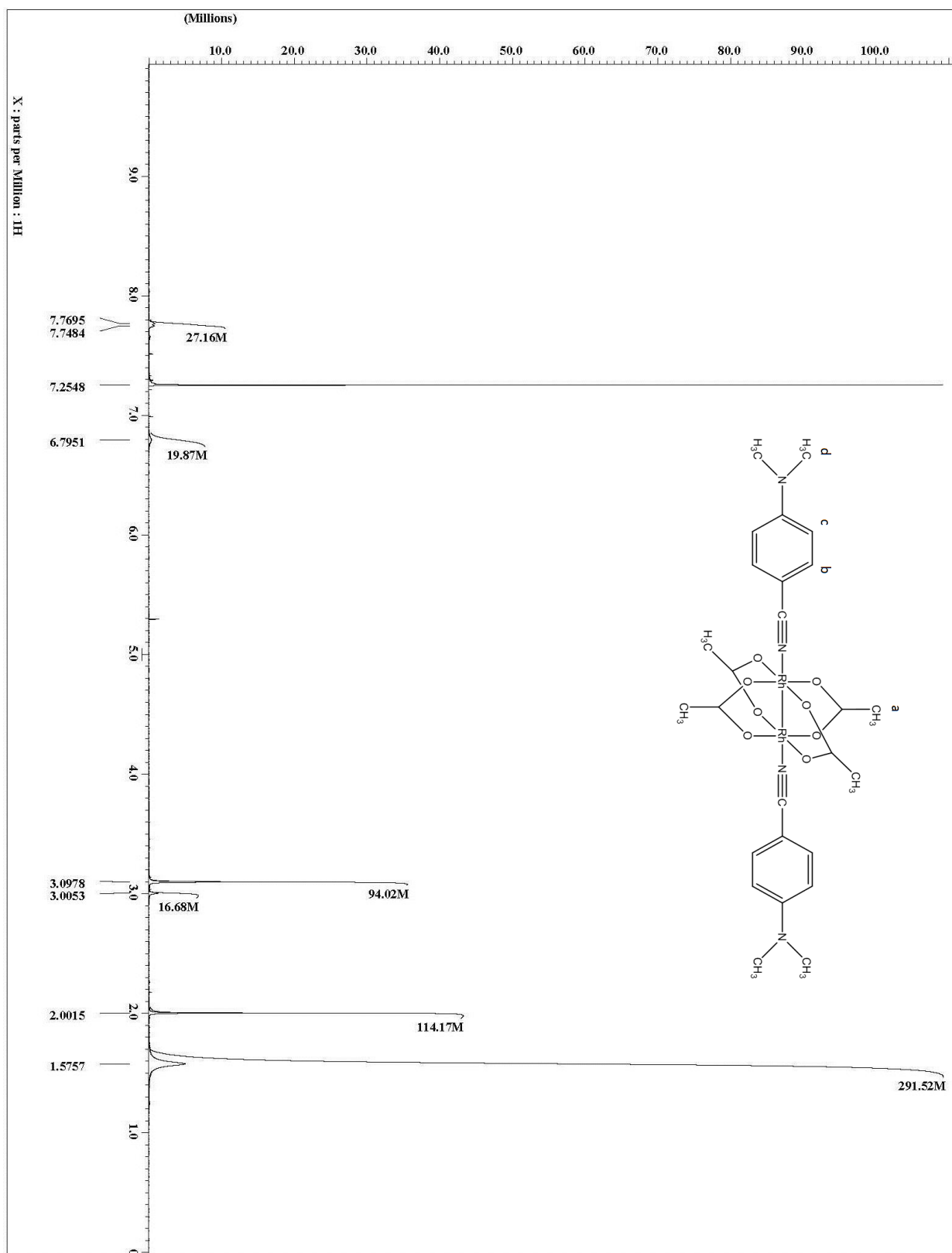
Figure 32: NMR spectrum of the 4-(dimethylamino)benzonitrile adduct.
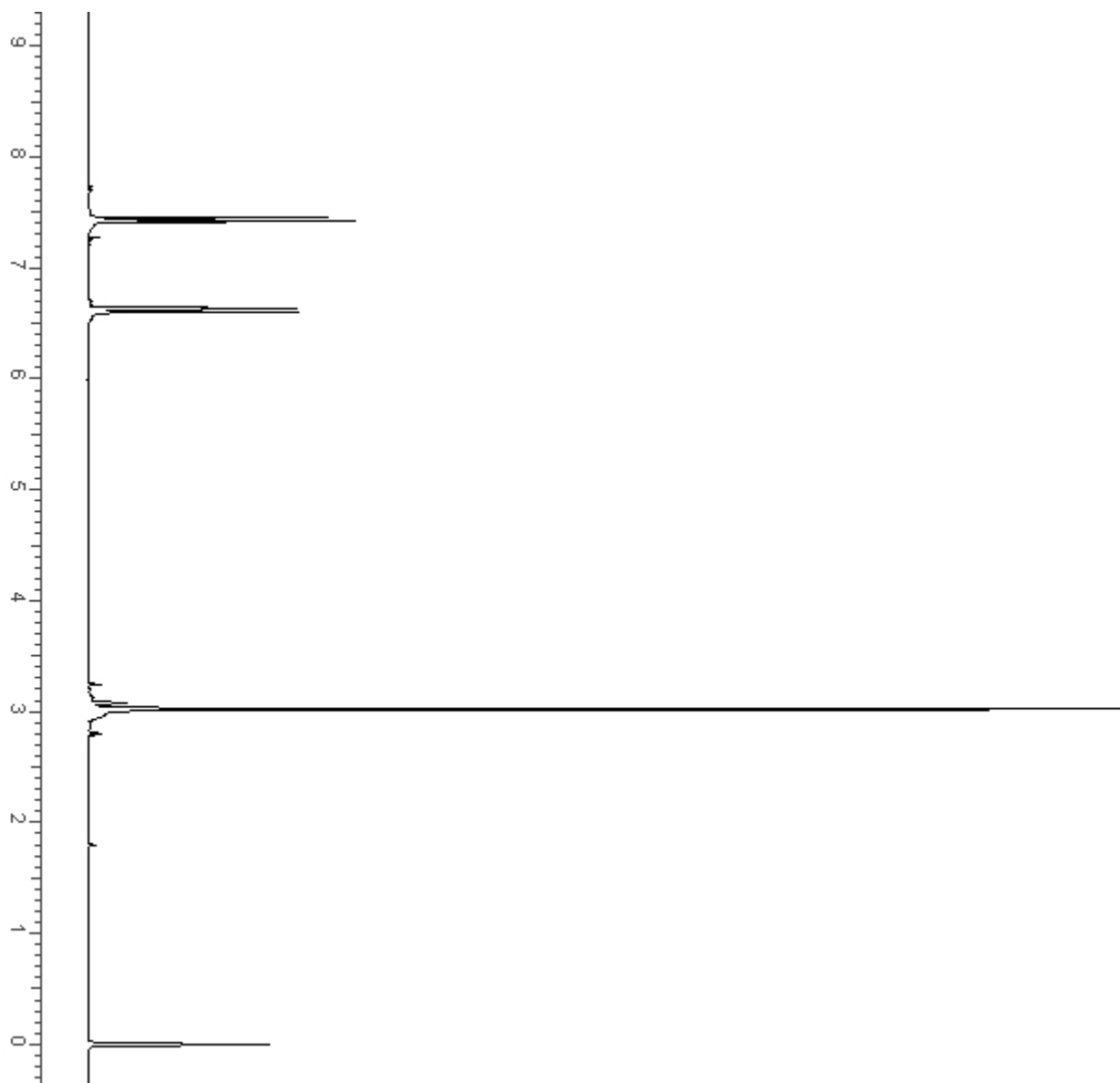
Figure 33: Literature NMR spectrum of 4-(dimethylamino)benzonitrile.[22]

Figures 34 and 35 show the 3,5-dinitrobenzonitrile adduct and unreacted 3,5-dinitrobenzonitrile, respectively. Based on the crystal structure, five peaks would be expected for the adduct: one from the methyl group from the equatorial ligands on the rhodium complex, two from the phenyl ring of the axial ligand, and two from the ethanol molecule that had reacted with the nitrile carbon. These peaks are assigned a, b, c, d, and e. In Figure 34 there are approximately six peaks, including the chloroform peak at δ 7.2548 and water at δ 1.5885. The methyl peak

55

from the acetate ligands, a, is thus located at δ 1.8312. When Figures 34 and 35 are compared, there are two sharp peaks at approximately δ 9.29 and δ 8.88 in the unreacted 3,5-dinitrobenzonitrile that correspond to the peaks at δ 9.1543 and δ 8.5639, respectively, labeled b and c. There also appears to be a peak at δ 4.6071, which could correspond to either the methyl or methylene hydrogens on the ethanol. Unfortunately, the peaks were weak, indicating a low concentration in the NMR tube. This limits the ability to discern all of the peaks, especially those on the ethanol. In regards to peaks labelled b and c, they both have shifted upfield by δ 0.15 and δ 0.32, respectively. This shift upfield is different from what was observed in the other spectrum, perhaps because of the ethanol molecule reacting to the nitrile carbon. The rehybridization of the carbon atom has changed the geometry of the benzonitrile: this effect and the attachment of the oxygen atom likely has a substantial impact on the shielding of the hydrogen atoms. Also, in comparison with the other NMR spectrum, peak a is approximately δ 0.2 farther upfield, indicating that the shielding effect is not exclusive to the axial ligand. This shielding of peaks a, b, and c still indicates a reaction; however, a reaction different from that experienced by the other adducts, which is reasonable based on the crystal data.
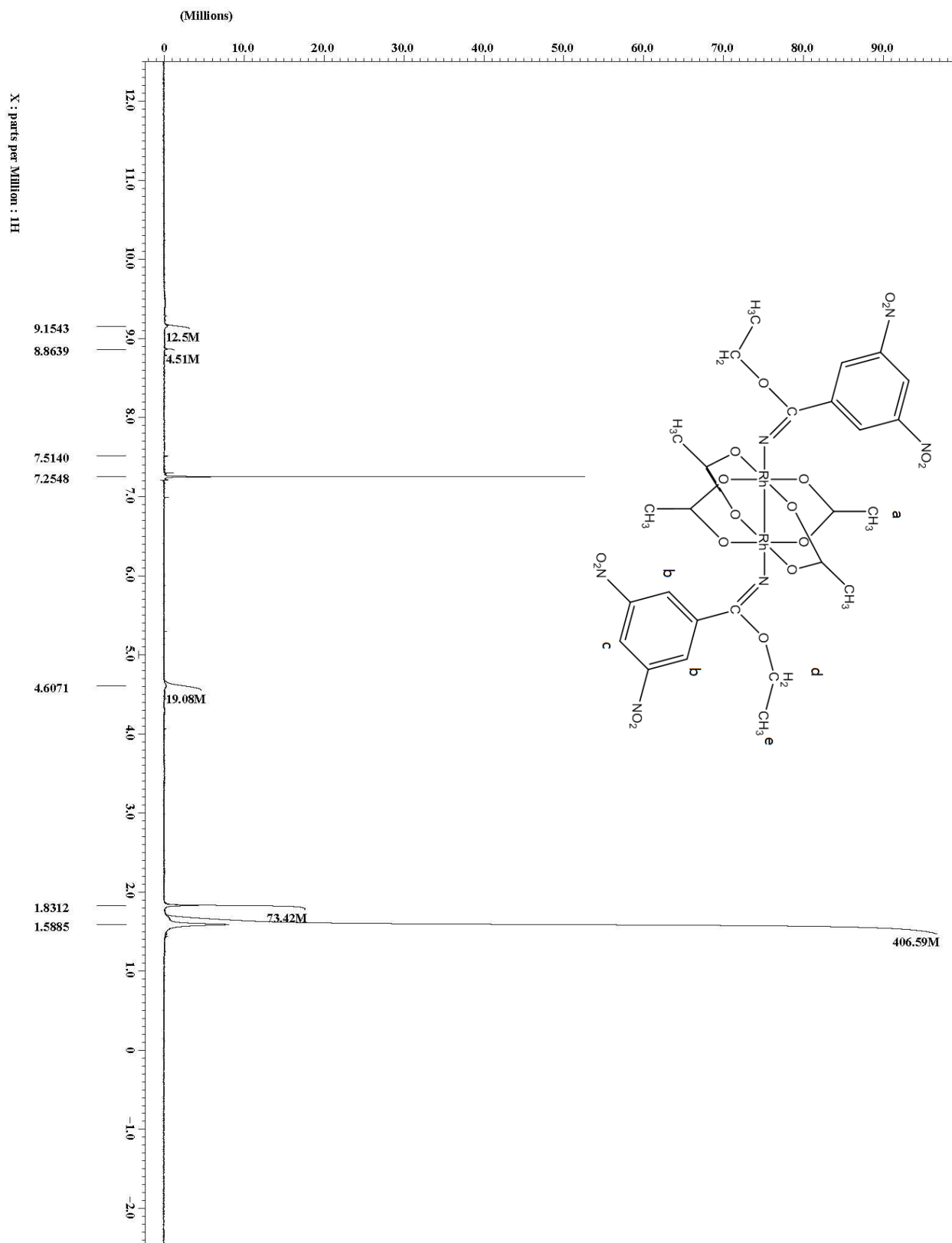
Figure 34: NMR spectrum of the 3,5-dinitrobenzonitrile adduct.
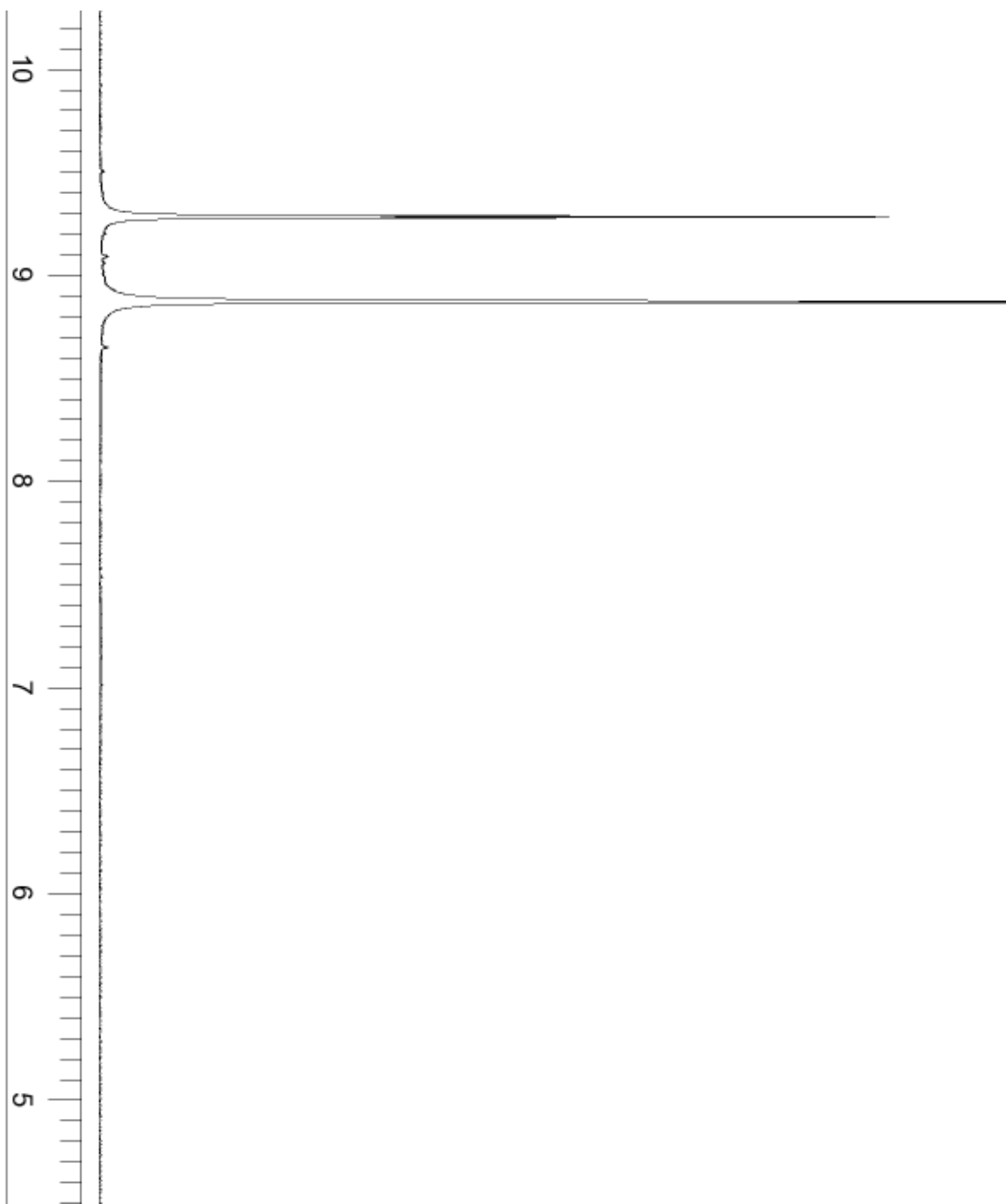
Figure 35: Literature NMR spectrum of 3,5-dinitrobenzonitrile.[23]

4. Conclusion

Four of the six proposed adducts of functionalized benzonitriles and rhodium acetate,

[Rh$_2$(COOCH$_3$)$_4$]·2NCC$_6$H$_4$NO$_2$, [Rh$_2$(COOCH$_3$)$_4$]·2NCC$_6$H$_4$NH$_2$,

[Rh$_2$(COOCH$_3$)$_4$]·2NCC$_6$H$_4$N(CH$_3$)$_2$, and [Rh$_2$(COOCH$_3$)$_4$]·2NCOCH$_2$CH$_3$C$_6$H$_3$(NO$_2$)$_2$, were

successfully prepared and characterized by X-ray crystallography. The structures all had low R$_1$

values, ranging from 0.0259-0.0416, indicating accurate models. All of the models indicated a nonlinear rhodium-nitrogen-carbon bonding, ranging from 173.80-179.02º, which does not support the classical definition of π-backbonding, although the 4-aminobenzonitrile adduct was the closest to linearity. An interesting development was the discovery that the ethanol molecule had reacted to the nitrile carbon in the 3,5-dinitrobenzonitrile adduct.

The significance of this study comes from the use of benzonitriles as carbene analogs in order to observe π-backbonding. One possibility for observing nonlinear bonding angles in the benzonitrile adducts is that the π-backbond is weak and cannot form due to the steric hindrance of the functionalized benzonitrile in the crystalline lattice, forcing bonding at an angle, or due to close contacts or intermolecular forces of the benzonitriles on nearby adducts. Eagle's work involving isonitrile adducts of rhodium acetate also produced structures that did not have linear bonding angles; however, it was argued that π-backbonding occurred due to the coplanarity of the benzene rings.[15] This leads to the need for the analysis of the coplanarity of the benzonitrile adducts in this study. This can be done with the structural software used in solving the adducts. It is recommended that other isonitrile analogs be used having the same functional groups as in this study, including nitro and amino groups, in order to observe bonding angles as well as coplanarity. Isonitriles are less stable than nitriles, however, so this analog would have to be prepared immediately before study.

In the IR analysis, similar wavenumbers were found in the nitrile region for all adducts, with two distinct peaks at 2378.23 and 2310.72 cm^{-1}. This maintains the successful attachment of nitrile to the rhodium complex. Another step forward would be to assign the specific stretches for the nitrile as dictated by symmetry. This requires using group theory. For the NMR data, literature peaks for the benzonitriles were compared to the data collected, indicating that the

benzonitriles were bound to rhodium acetate in the solution phase. For the 4-nitrobenzonitrile and the 4-(dimethylamino)benzonitrile adducts of rhodium acetate, peaks for the benzonitrile were shifted downfield, indicating a loss of electron density around those hydrogens, while the 3,5-dinitrobenzonitrile adducts indicated that peaks were shifted upfield, indicating a gain of electron density, likely because of the Pinner reaction. For future NMR analysis, more of the adducts could be synthesized in order to obtain a stronger signal. This would allow better integration of the peaks in each spectrum.

The 3,5-diaminobenzonitrile adduct of rhodium acetate initially produced a red amorphous precipitate and over several months this solid reentered solution. This made the case for a kinetic and thermodynamic product, and the thermodynamic product should be able to be crystallized by the vapor diffusion method used for the four adducts in this study. While the 3,5-diaminobenzonitrile adduct of rhodium acetate will be studied crystallographically in the future by the Eagle group, an experiment should be conducted in order to explain the formation of the kinetic and thermodynamic product. An initial step would be to analyze the precipitate initially formed, believed to be the kinetic product, by IR and NMR spectroscopy and compare the results to the data collected on the other benzonitrile adducts, as well as to the thermodynamic product.

The 3,5-dinitrobenzonitrile adduct of rhodium acetate formed a structure that was not predicted. The solvent, ethanol, reacted with the carbon atom of the nitrile to form a bond, which was subsequently found in the crystalline lattice. The reaction likely occurred because of the nitro groups attached to the benzene ring, which are strongly electron withdrawing. Therefore, this adduct needs further experimental work. Because the NMR spectrum presented here showed very small peaks, it is recommended that a more concentrated solution be tested. This could help determine if the hydrogen found on the ethanol molecule remained attached and that zwitterion

was the product. The solvent used should be anhydrous because the nucleophilic water could abstract this hydrogen atom. Another study for this adduct would be to dissolve a large amount of the adduct into water and test the solution's acidity, with a pH decrease indicating that water did abstract the hydrogen atom.

References

1. Doyle, M. P. "Perspective of dirhodium carboxamidates as catalysts." *Journal of Organic Chemistry*, **2006**, *71*, 9253-9260.
2. Paulissenen, R.; Reimlinger, H.; Hayez, E.; Hubert, A. J.; Teyssie, P. "Transition metal catalyzed reactions of diazocompounds- II insertion in the hydroxylic bond." *Tetrahedron Letters*, **1973**, *24*, 2233.
3. Doyle, M.P. "Control of enantioselectivity in catalytic metal carbene reactions." *Enantiomer*, **1999**, *4* (6), 621-632.
4. Davies, H.; Beckwith R. "Catalytic Enantioselective C-H Activation by Means of Metal-Carbenoid-Induced C-H Insertion." *Chemical Reviews,* **2003**, *103,* 2861-2903.
5. Dennis, A. M.; Korp, J. D.; Bernal, I.; Howard, R. A.; Bear, J. L. "Crystal and molecular structure of the bis(pyridine) adduct of a dinuclear rhodium(II) complex with trifluoroacetamidato bridging ligands." *Inorganic Chemistry,* **1983**, *22*, 1522-1529.
6. Doyle, M. P.; Brandes, B. D.; Kazala, A. P.; Pieters, R. J.; Jarstfer, M. B.; Watkins, L. M.; Eagle, C. T. "Chiral rhodium(II) carboxamides. A new class of catalysts for enantioselective cyclopropanation reactions." *Tetrahedron Letters*, **1990**, *31* (46), 6613-6616.
7. Eagle, Cassandra T.; Farrar, David G.; Holder, Grant N.; Pennington, William T.; Bailey, Rosa D. "Structural and Electronic Properties of (2,2-trans)-Dirhodium(II) Tetrakis(N-phenylacetamidate)." *Journal of Organometallic Chemistry,* **2000**, *596,* 90-94.
8. Yates, P. "The Copper-catalyzed Decomposition of Diazoketones." *Journal of the American Chemical Society,* **1952**, *74*, 5376.
9. Doyle, M. P. "Catalytic Methods for Metal Carbene Transformations." *Chemical Reviews*, **1986**, *86*, 919-939.
10. Casey, C. P.; Polichnowski, S. W.; Shusterman, A. J.; Jones, C. R. "Reactions of Benzylidene Pentacarbonyltungsten with Alkenes." *Journal of the American Chemical Society*. **1979**, *101*, 7282.
11. Miessler, G.L.; Fischer, P.J.; Tarr, D.A. "Molecular Orbitals from d Orbitals." *Inorganic Chemistry,* 5th ed.; Pearson Education, Inc.: Upper Saddle River, NJ, **2014**, 121-122.
12. Cotton F. A. Rhodium Compounds. Multiple Bonds Between Metal Atoms. 3rd ed.; Springer Science and Business Media, Inc.: New York, NY, **2005**, Chapter 12.
13. Cotton, F. A.; Thompson, J. L. "The structure of tetra-μ-acetato-bis(acetonitrile)dirhodium(II)(*Rh-Rh)*." *Acta Crystallographica,* **1981**, *B37*, 2235-2236.
14. Eagle, C. T.; Quarshie, F.; Ketron, M. E.; Atem-Tambe N. "*cis*-Tetrakis(μ-*N*-phenylacetamidato)-κ^{4}N:O;κ^{4}O:N-bis[(benzonitrile-κN)rhodium(II)](*Rh-Rh)*." *Acta Crystallographica,* **2013**, *E69*, m329.
15. Eagle, C.T.; Farrar, D.G.; Plaff, C.U.; Davies, J.A.; Kluwe, C.; Miller, L. "π-Back-Bonding in Bis(isonitrile) Complexes of Rhodium(II) Acetate: Structural Analogs for Rhodium Carbenoids." *Organometallics*, **1998**, *17*, 4523-4526.
16. McMurry, John. "Substituent Effects in Substituted Aromatic Rings." *Organic Chemistry,* 8th ed.; Brooks Cole: Belmont, CA, **2012,** Chapter 16.
17. Sands, D. E. Introduction to Crystallography. Dover Publications, Inc.: Mineola, NY, **1993**.
18. Skoog, D.A.; Holler, J.F.; Crouch, S.R.: "Diffraction of X-rays and Bragg's Law." *Principles of Instrumental Analysis.* 6th Edition; Brooks/Cole, Cengage Learning: Belmont, CA, **2007**, 309-310.

19. Roger, R.; Neilson, D.G. "The Chemistry of Imidates." *Chemical Reviews*, **1961**, *61*, 179-211.
20. Pinner, A.: *Die Imidöather und ihre Derivate*. Oppenheim, Berlin, **1892**.
21. SciFinder; Chemical Abstracts Service: Columbus, OH; NMR Spectrum of 4-nitrobenzonitrile; Spectrum ID N12007.h; RN 619-72-7; http://scifinder.cas.org (accessed February 26, 2015).
22. SciFinder; Chemical Abstracts Service: Columbus, OH; NMR Spectrum of 4-(dimethylamino)benzonitrile; Spectrum ID D139505.h; RN 1197-19-9; http://scifinder.cas.org (Accessed February 26, 2015).
23. SciFinder; Chemical Abstracts Service: Columbus, OH; NMR Spectrum of 3,5-dinitrobenzonitrile; Spectrum ID WHSP44505; RN 4110-35-4; http://scifinder.cas.org (Accessed February 26, 2015).

Appendix

File Locations of Solved Crystal Structures on Eagle Group's Computer:

1. 4-nitrobenzonitrile adduct of rhodium acetate
    Jared -> Rh2(OAc)4_4-NitroPhCN_solved_reinheimer

2. 4-aminobenzonitrile adduct of rhodium acetate
    Jared -> Rh2(OAc)4_4-Aminobenzonitrile_EtOH_H2O_B_renumbered

3. 4-(dimethylamino)benzonitrile adduct of rhodium acetate
    Jared -> Rh2(OAc)4_4-dimethylaminoPhCN_EtOH_H2O_renumbered

4. 3,5-dinitrobenzonitrile adduct of rhodium acetate
    Jared -> Rh2(OAc)4_3_5-dinitroPhCN_EtOH-MeOH_C_renumbered

Also, a folder located on the desktop titled "Jared Publication Materials" contains CIF files, packing diagrams, and X-ray Structure Reports for some of the above structures.

Contact Information:

University email: LOWEJM1@goldmail.etsu.edu